Check for updates

JGR Planets

RESEARCH ARTICLE
10.1029/2022JE007207

Key Points:

- We identified 360 known and suspected volcanic cones in the Marius Hills region using high-resolution topography and image data
- Geomorphometric characterization of these cones indicates various eruption styles
- The cones in Marius Hills are smaller than lunar domes, suggesting low-volume and small-scale eruptions

Supporting Information:

Supporting Information may be found in the online version of this article.

Correspondence to:

L. Qiao and Z. Ling,
leqiao.geo@gmail.com;
zcling@sdu.edu.cn

Citation:

Wan, S., Qiao, L., & Ling, Z. (2022). Identification and geomorphometric characterization of volcanic cones in the Marius Hills, the Moon. *Journal of Geophysical Research: Planets*, *127*, e2022JE007207. https://doi.org/10.1029/2022JE007207

Received 26 JAN 2022
Accepted 3 OCT 2022

Author Contributions:

Conceptualization: Zongcheng Ling
Data curation: Sheng Wan
Formal analysis: Sheng Wan, Le Qiao, Zongcheng Ling
Funding acquisition: Zongcheng Ling
Investigation: Sheng Wan, Le Qiao, Zongcheng Ling
Methodology: Sheng Wan, Le Qiao, Zongcheng Ling
Project Administration: Zongcheng Ling
Resources: Le Qiao, Zongcheng Ling
Software: Sheng Wan, Le Qiao
Supervision: Le Qiao, Zongcheng Ling
Validation: Sheng Wan, Le Qiao, Zongcheng Ling
Visualization: Sheng Wan, Le Qiao
Writing – original draft: Sheng Wan
Writing – review & editing: Sheng Wan, Le Qiao, Zongcheng Ling

© 2022. American Geophysical Union. All Rights Reserved.

Identification and Geomorphometric Characterization of Volcanic Cones in the Marius Hills, the Moon

Sheng Wan[1], Le Qiao[1], and Zongcheng Ling[1]

[1]Shandong Key Laboratory of Optical Astronomy and Solar-Terrestrial Environment, School of Space Science and Physics, Institute of Space Sciences, Shandong University, Weihai, China

Abstract Investigation of the detailed geological characteristics of lunar volcanic cones can peer into their formation and emplacement processes, thus deepening our understanding of pyroclastic eruptions on the Moon. In this work, we focus on the Marius Hills region (centered at 13°N, 55°W), a volcanic plateau in south Oceanus Procellarum, which hosts the most abundant volcanic cones on the Moon, along with other volcanic features. The range of volcanic features indicates various eruption styles and complicated sequences of regional magmatic activities. Based on the SLDEM2015 topography data, with assistance from other multisource topography and image data sets, we identified 360 known and suspected volcanic cones and 22 volcanic domes in the Marius Hills. Following detailed morphological characterizations, the volcanic cones show various morphology types, including *C-shaped*, *elliptical-shaped*, *elongated-shaped*, *irregular-shaped*, and *rounded-shaped*. The cones (median basal width ~2.7 km, height ~115 m, and volume 0.25 km^3) contain summit pit craters (15%; median width ~358 m), exhibiting smaller basal widths and summit pit crater widths compared with lunar mare domes. The mean slope (3.5°–15.6°) and rock abundance (0.3%–3.8%) of volcanic cones in Marius Hills are larger than those of the mare dome, suggesting different eruption mechanisms. Marius Hills cones also show larger basal widths and smaller height/width ratios than terrestrial volcanic cones, which are attributed to multiple factors, including subaerial environment, volatile content of the magma, eruption rate, and lava viscosity.

Plain Language Summary Volcanism is one of the major geological processes of the Moon. Studying the geological characteristics of lunar volcanic features is of significant scientific value to provide important insights into the geological and thermal evolution history of the Moon. Lunar volcanic cones, conical-shaped mounds occasionally with summit pit craters, are typically interpreted to represent explosive eruption. Here, we conducted a detailed geomorphology study of the volcanic features around the Marius Hills region (centered at 13°N, 55°W) on the Moon using the latest high-resolution topography and image data. We identified 360 known and suspected volcanic cones in this region. Geomorphometric characterization of these cones indicates various eruption styles. We find that the cones in Marius Hills are smaller than lunar domes, suggesting low-volume and small-scale eruptions. Lunar cones are larger and shorter than terrestrial cones, mainly attributed to the effects of unique lunar environments. The measurement and analyses of their morphologies enhance our understanding of the history of lunar volcanism.

1. Introduction

Volcanism is one of the main geological processes on terrestrial bodies and produces various volcanic features, including volcanoes of specific shapes, pyroclastic deposits, and lava flows. Volcanoes are the surface manifestations of thermal activity and magmatism of the parent planet. Different volcanic landforms are important indicators of various eruption processes. Investigations of the geomorphologies of volcanoes can provide key information for constraining the magma source region properties, eruption types, and emplacement processes (e.g., Thouret, 1999).

Cinder cones, typically a few hundred meters in diameter and tens to hundreds of meters tall (Earle, 2019), are among the most common volcanic structures on Earth. These steep conical hills are generally interpreted to be built from loose pyroclastic fragments when bubble-rich magma lava is ejected violently from the eruption vent, which breaks up into small drops, solidifies, and finally falls back around the vent to form circular or elliptical cones of cinders, clinkers, or scoria (e.g., Poldervaart, 1971).

Volcanic cones have also long been observed on the Moon. Due to the unique physical environment of the Moon, including the low gravity and the lack of an atmosphere, cones formed on the Moon are broader and lower than those formed on Earth (e.g., Wilson & Head, 1981). Lunar volcanic cones are generally conical-shaped mounds occasionally with summit pit craters. Previous studies have utilized high-resolution Lunar Orbiter and Apollo photographic images to study the spatial distribution and morphology of lunar cones. Guest and Murray (1976) described lunar cones as typically 2–3 km across at the base with summit craters 0.5–1 km in diameter and among the most common volcanic landforms on the Moon. These cones were found in local clusters or scattered forms in mare units (Greeley, 1971; Heather et al., 2003; Lawrence et al., 2013; Weitz & Head, 1999; Whitford-Stark & Head, 1977). According to their morphological and topographic characteristics, Head (1975) classified volcanic landforms into three types: Dark halo craters, small cones, and large cones. Some lunar cones with associated lava flows were interpreted to represent volcanic eruptions of magma of relatively high volatile contents (Whitford-Stark & Head, 1977). While some lunar cones without associated lava flow, for instance, the Rima Parry cone chain, were thought to be formed by the degassing of a near-surface dike producing both spatter and volcanic glasses (Weitz & Head, 1999). Lawrence et al. (2013) utilized the Lunar Reconnaissance Orbiter Camera (LROC) data sets to investigate the morphology and distribution of abundant volcanic cones in Marius Hills and classified them into various types, including C-class, E-class, N-class, and U-class. However, due to the very limited coverage of high-resolution topography data (decameter pixel size or finer; LROC NAC DTM in the case of Lawrence et al. (2013)), detailed topographic characteristics of lunar cones are poorly analyzed and some cones were probably missed. Using Clementine multispectral maps, Weitz and Head (1999) found that most volcanic cones in the Marius Hills have weaker mafic absorptions than the adjacent mare deposits and volcanic domes, while the Isis and Osiris cones in southern Mare Serenitatis are spectrally similar to adjacent mare units. Using the same data, Heather et al. (2003) inferred that cones on the Marius plateau were dominated by a strong glassy signature and often had associated microlithic structures. Besse et al. (2011) analyzed the Moon Mineralogy Mapper (M^3) data of Marius Hills cones and found that they belonged to the high-calcium pyroxene plateau unit and might contain more silica and opaque minerals, while less olivine.

Lunar volcanic cones have been previously identified mainly from orbital photographs (Guest & Murray, 1976; Lawrence et al., 2013; Weitz & Head, 1999; Whitford-Stark & Head, 1977). However, due to the small sizes and very gentle topographic reliefs of some lunar volcanic cones, many of them are not easily identified, especially under the condition of low sun illumination or obscured by other surface features. New high-resolution altimetric data, especially the Kaguya Terrain Camera (TC) stereogrammetry digital terrain model (DTM; 10 m/pixel and ∼3–4 m altimetric accuracy; Haruyama et al., 2012) and the blended LOLA/Kaguya TC topography (SLDEM2015; 512 pixels/degree spatial resolution and ∼3–4 m vertical accuracy; Barker et al., 2016) provide an excellent basis for discovering and characterizing geomorphic features on the Moon, including volcanic cones.

As one of the largest single concentrations of volcanic features on the Moon (Weitz & Head, 1999; Whitford-Stark & Head, 1977), the Marius Hills are undoubtedly the best place for lunar cone studies. With assistance from multisource data sets, we carried out a comprehensive search campaign for volcanic cones in Marius Hills to deepen the understanding of lunar volcanism.

2. Data and Methodology

We first established the criteria for the identification of volcanic cones in the Marius Hills based on previously identified cones. We then conducted a systematic search of volcanic cones in Marius Hills using mainly Kaguya TC DTM and SLDEM2015 topography. Building on previous investigations (Lawrence et al., 2013), we recognized five shape types for volcanic cones in Marius Hills: Letter *C-shaped*, *elliptical*, r*ounded*, i*rregular*, and e*longated*. We employ rock abundance data (∼500 m/pixel) derived from Diviner thermophysical data (Bandfield et al., 2011) to characterize the concentration of blocks near volcanic cones. Kaguya TC image mosaic (∼10 m/pixel) was used for regional geologic context and geomorphological analyses.

The Kaguya DTM topography employed in this work is the high-resolution (10 m/pixel) that covers the entire Marius Hills region. This data set is not available in previous works (e.g., Lawrence et al., 2013), thus hampering topographic analyses of all cones in the Marius Hills. For instance, Lawrence et al. (2013) used the GLD DEM topography (Scholten et al., 2012), which indeed covers the entire studied region, but its resolution (100 m) is too coarser to characterize many small cones. Lawrence et al. (2013) also used the LROC NAC DTM topography, which is true of very high resolution (2 m), while it only comes from a tiny part of the studied area. We use the

Kaguya TC DTM topography data to investigate the topographic characteristics of each cataloged volcanic cone. High-resolution and high-precision topography data enable us more detailed and accurate morphometric analysis of cones in Marius Hills. The basal width (W_{co}), ellipticity, height (H_{co}), area, volume (V_{co}), and slope (mean slope across the cone) (Grosse et al., 2012) are measured or calculated to analyze morphological characteristics of volcanic edifices. For some cones with summit craters, the width (W_{cr}) and depth (D_{cr}) of the summit crater are also measured. Some basic morphological data are defined as follows:

$$W_{CO} = \sqrt{ab} \tag{1}$$

$$H_{co} = H_{max} - H'_{mean} \tag{2}$$

$$V_{co} = S_{co}\left(H_{mean} - H'_{mean}\right) \tag{3}$$

where a and b are the length and width of the smallest bounding rectangle of each volcanic cone, respectively, H_{max} is the maximum elevation of the cone, H'_{mean} is the mean elevation of the surrounding terrain (a buffer zone with a width of W_{co} * 20%) of the volcanic cone, S_{co} is the surface area of the volcanic cone, and H_{mean} is the mean elevation of the cone. Some morphological ratio parameters (H_{co}/W_{co}, W_{cr}/W_{co}) are calculated to characterize the topographic profiles of cones. Moreover, we used histograms (Figures 8a, 8b, 9a, 9b, 10a, 10b, 11a, 13a, 14a and 14b) to show the distribution of morphological parameters and morphometric ratios (Figures 9c, 10c, 11b, 13d, 13e, 14e, and 14f) of volcanic cones of different shapes and scatter plots to explore the potential relationship between different morphological parameters.

3. Geologic Context of the Marius Hills

The Marius Hills complex is a volcanic plateau centered at ~13.4°N, 55.6°W in the southern Oceanus Procellarum. It is ~390 × 300 km in size, with a surface area of ~117,000 km^2 (Figure 1a). Abundant volcanic features (domes, cones, sinuous rilles, and collapse pits) occur on it, indicating intense volcanic activities of various eruption styles, whose ages range from 3.3 to 3.8 Ga (Greeley, 1971; Imaeda et al., 2013; Lawrence et al., 2013; McCauley, 1967, 1968; Weitz & Head, 1999; Heather et al., 2003; Whitford-Stark & Head, 1977). Six west-east and north-south topographic profiles crossing the Marius Hills are mapped in Figure 1c to characterize the complex terrain. This volcanic plateau rises about 1.2 km from the surrounding maria (Figure 2), which results from high-volume eruptions that formed a large shield.

Whitford-Stark and Head (1980) proposed that the Marius Hills complex may be a major source for the Hermann Formation, a very extensive volcanic deposit emplaced in southwestern Oceanus Procellarum. McCauley (1967) mapped hundreds of mare domes in Marius Hills and classified them into low domes (typically 2–3° in slope) with smooth surface textures, steep domes (typically 6–7°) with rugged surfaces, and small-dome clusters. Guest and Murray (1976) identified many pyroclastic cones in Marius Hills and interpreted them as conical-shaped mounds with summit craters. These cones and domes on Marius Hills were measured as up to 20 km in diameter and ~200–600 m in height. Many sinuous rills were also identified in the area, often associated with irregular or slender vents (Greeley, 1971; Guest, 1971; McCauley, 1967). Using Lunar Orbiter images, Whitford-Stark and Head (1977) identified 20 sinuous rilles, 135 low domes, 127 steep domes, and 59 volcanic cones in Marius Hill, while Weitz and Head (1999) identified 121 domes and 46 volcanic cones in the Marius Hill. Lawrence et al. (2013) use LRO data to reexamine the geology of the volcanic domes, cones, and related depression features. Compared with previous statistics, additional 56 volcanic features were identified. The wide range of volcanic features, from broad low domes to steep cones, indicates a range of variable eruption conditions (Lawrence et al., 2013).

Prior studies have also revealed many compositional characteristics of the Marius Hills region. Sunshine et al. (1992) analyzed the Galileo spectrometer data and defined two high-Ti units in this region. Weitz and Head (1999) used the Clementine ultraviolet-visible (UVVIS) camera data to identify a mare unit with a high Ti content and found that mare domes in Marius Hills were spectrally identical to the adjacent mare, while the volcanic cones were characterized by lower reflectance and weaker mafic absorptions. Heather et al. (2003) mapped the lava flows in Marius Hills and found that the Marius Hills region was dominated by high-Ti Eratosthenian basalt, with a range of emplacement ages and compositions. In addition, the cones on the Marius plateau were dominated by a strong glassy signature and often have an associated microlitic structure (Heather

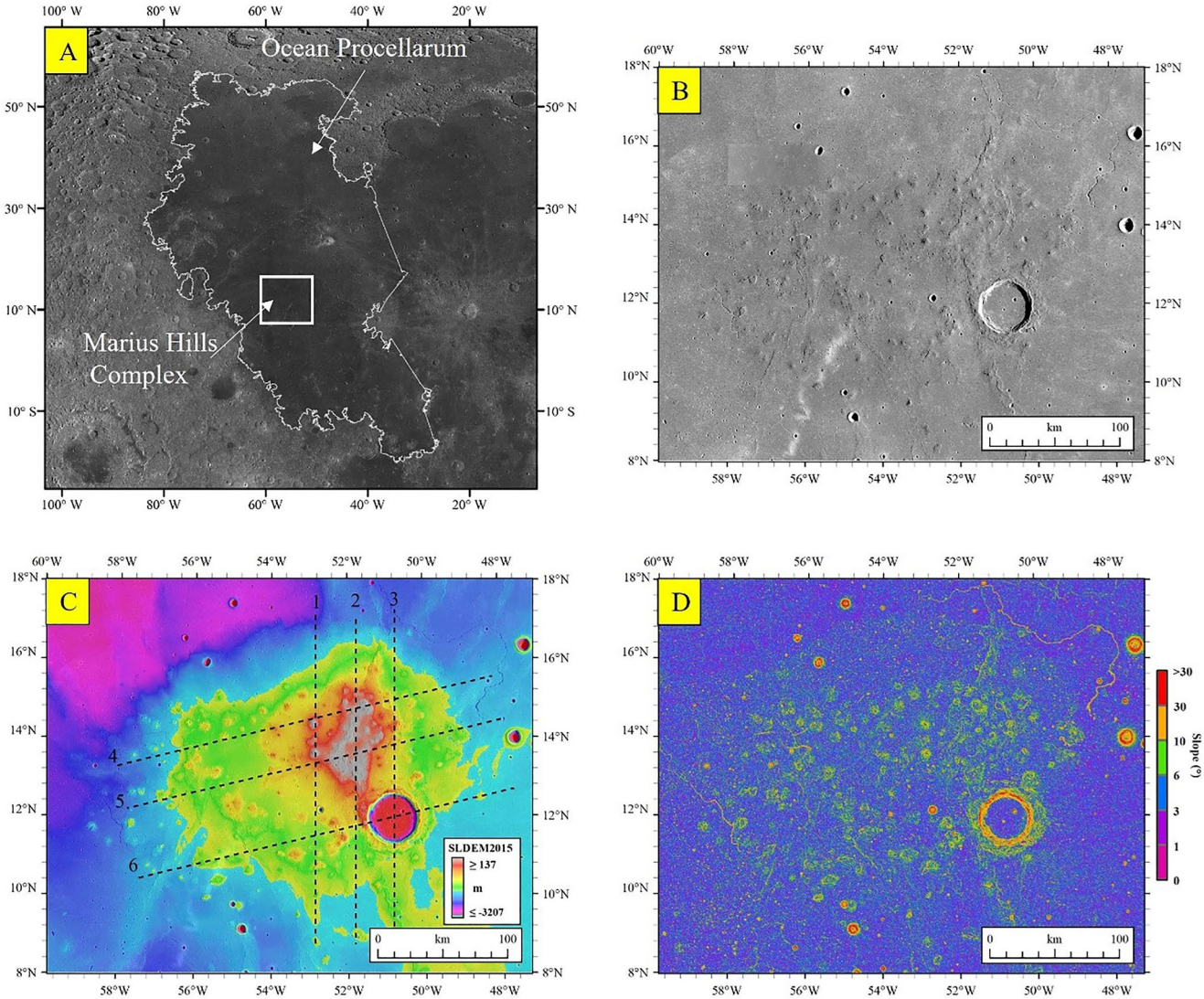


Figure 1. The regional context of the Marius Hills. (a) Lunar Reconnaissance Orbiter Camera Wide-Angle Camera low-Sun mosaic (100 m/pixel), marking the location of the Marius Hills in Oceanus Procellarum (Nelson et al., 2014), (b) Kaguya Terrain Camera (TC) morning mosaic, and (c) SLDEM2015 topography (~60 m horizontal resolution). The black dotted lines mark the locations of topographic profiles shown in Figure 2, with their starting points labeled by the profile numbers. (d) Kaguya TC digital terrain model-derived slope.

et al., 2003). Besse et al. (2011) analyzed the Moon Mineralogy Mapper (M^3) data of this region and classified regional mare basalts into two groups: Olivine-rich basalts and basalts with a high-calcium pyroxene-dominated composition. Arya et al. (2014) found that the mare dome in Marius Hills was enriched in mafic mineralogy with dominant high-calcium pyroxene and high titanium but lesser iron. Olivine is depleted according to the IBD analysis. Moreover, Lawrence et al. (2013) analyzed the Diviner thermophysical data and found that regional mare domes are not rich in silica and are similar to surrounding mare deposits.

4. Identification of Volcanic Cones in Marius Hills

Volcanic cones are often observed to be related to surrounding volcanic features. Therefore, we conducted a systematic search for volcanic cone features in this region. Additional volcanic features, including domes and sinuous rilles, are also identified. In total, we identify 360 volcanic cones and 22 mare domes in the Marius Hills, they are mapped in Figure 7a. The classification of each cone and dome identification is also determined. We also

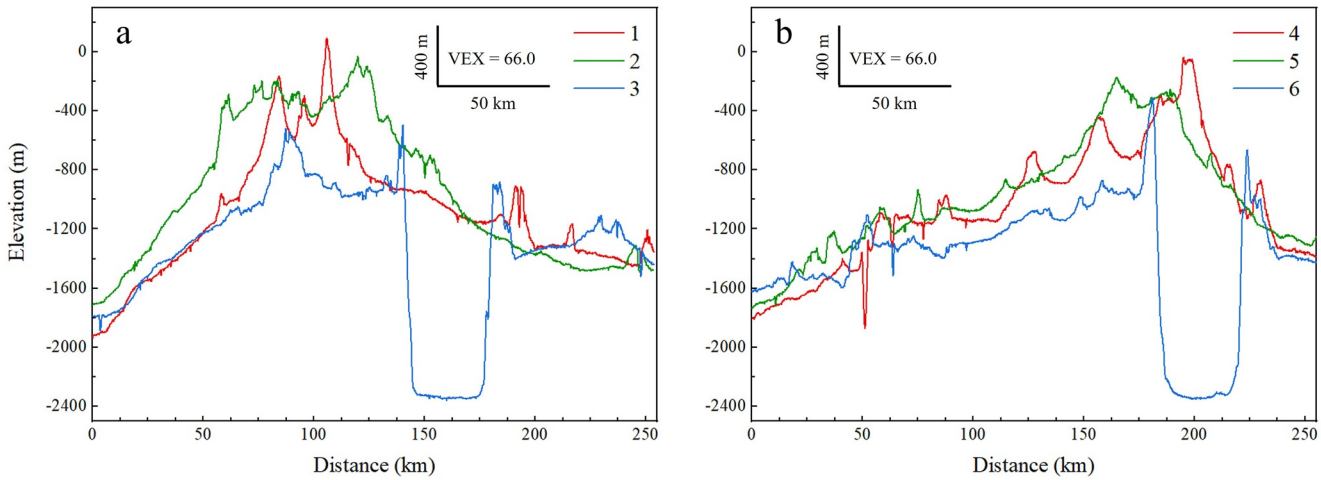


Figure 2. (a) West-east and (b) north-south topographic profiles crossing the Marius Hills complex, derived from SLDEM2015 topography, with vertical exaggeration (VEX) labeled. The locations of these profiles are shown in Figure 1b, and the profile numbers correspond to those shown there.

mapped the spatial distribution and density of volcanic cones. Moreover, we compared our identification results with those in previous studies.

4.1. Criteria and Classification for Identification of Volcanic Cones

We surveyed previously cataloged volcanic cones (Guest & Murray, 1976; Lawrence et al., 2013; Weitz & Head, 1999; Whitford-Stark & Head, 1977) and revealed some of their fundamental characteristics. We listed the following criteria for the identification of volcanic cones in Marius Hills, based on their topographical, geomorphological, and morphometrical characteristics: (a) A typical well-developed volcanic cone is characterized by a conical raised structure with a generally convex-shape and relatively steep (>10°) topographical slopes and a (quasi-) circular or elliptical outline; (b) lunar cones are often surrounded by other volcanic features (e.g., rilles, lava flows, domes, etc.); (c) the transition between cones and adjacent terrains is typically characterized by an obvious topographical slope change; and (d) surface textures of volcanic cones are typically rougher than typical mare plains and domes. Some cones occur in clusters and are difficult to distinguish individually, thus are designated as volcanic cone clusters. Summit pit craters are not present at many cones, thus they are not criteria for cone identification. But their occurrence will facilitate the identification and classification of the host cones.

The classification of each cone is determined as the following:

Definite volcanic cones (Class A): The characteristics of cones meet all criteria described above and the cone identity can be confirmed.

Possible volcanic cones (Class B): Cones in this class only meet parts of the criteria described above. The boundaries of some volcanic cones are apparent, with obvious uplift relative to the surrounding terrain but the surface lacks the rough textures of typical lunar cones. Alternatively, some cones are subject to some degree of topographical degradation, and the slope change along the edges is very subtle.

Questionable volcanic cones (Class C): The development of a volcanic cone is sometimes affected by preexisting topography or subsequent impacts; in these cases, the outline of the cone is poorly defined.

Figure 3 shows the spatial distribution of definite, possible, and questionable volcanic cones in Marius Hills.

4.2. Classification of Morphological Characteristics of Volcanic Cones in Marius Hills

We finally identified 216 volcanic cones (Class A) and 142 possible cones (Class B) in Marius Hill (Figure 6). These observations reconfirm that Marius Hills contain the highest density of volcanic cones across the Moon.

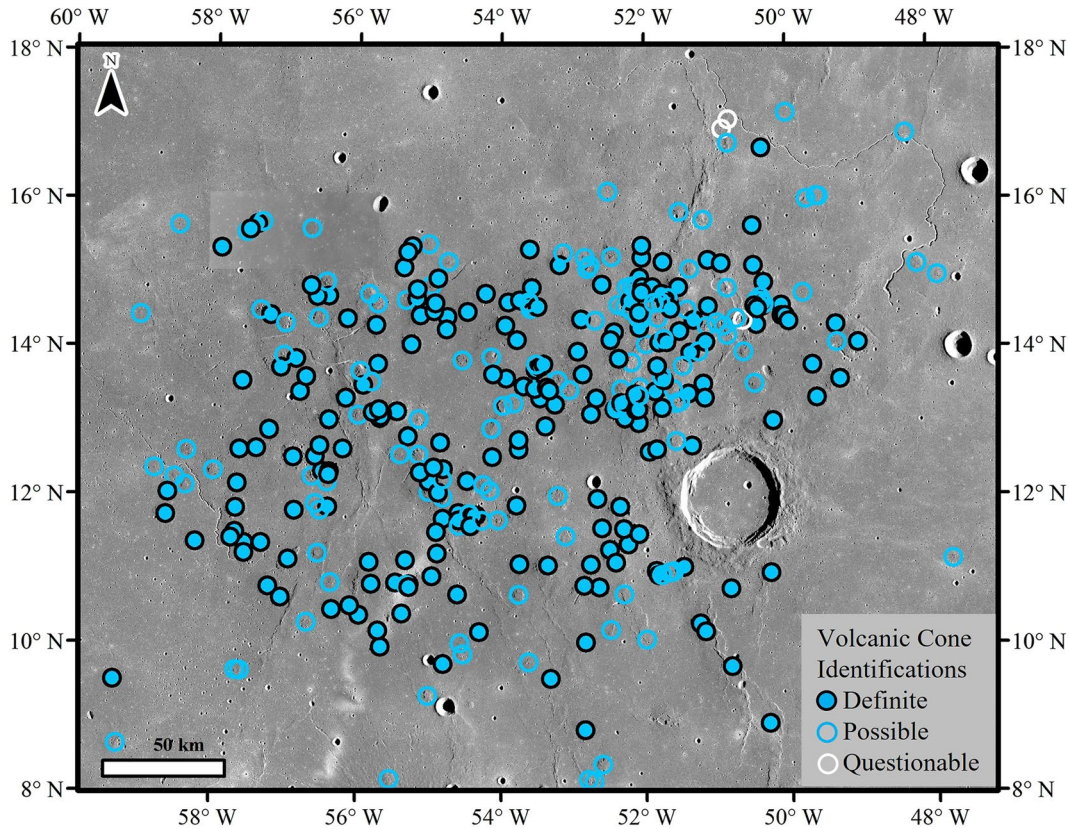


Figure 3. Spatial distribution of definite, possible, and questionable volcanic cones in Marius Hills.

Based on the geological characteristics of the Marius Hills cones presented here and in previous studies (e.g., Lawrence et al., 2013), we recognized the following shape types of cones:

Rounded cones: These (sometimes clustered) volcanic cones (Figures 4a and 4b) display a rounded outline, with an ellipticity typically less than 1.2. Due to the effect of preexisting topography or subsequent geological modifications, parts of the recognized volcanic cone boundaries are not standard circulars. These cones are classified as quasi-rounded (*r**) cones, while still cataloged into *rounded* cones in later statistics. In total, 75 rounded cones are identified.

Elliptical cones: These volcanic cones (Figures 4c and 4d) display an elliptical outline, with an ellipticity generally greater than 1.2. Similar to rounded cones described above, their outline shapes are also sometimes affected by preexisting topography or subsequent geological modifications, resulting in nonstandard ellipse shapes; they are designated as quasi-elliptical (*e**). We discovered 151 (quasi-) *elliptical* cones in this work.

Letter C-shaped cone: Due to the occurrents of opening in parts of the flank, these volcanic cones (Figures 4e and 4f) display the outline of letter C, previously described as a horseshoe appearance (Weitz & Head, 1999). The flank opening is commonly associated with at least one lobate lava flow. In total, 32 *C-shaped* cones were identified in this study. Lawrence et al. (2013) found 64 *C-class* cones in Marius Hills, while we only identify 32 C-shaped cones, mainly because many volcanic cones cataloged in this work are in clusters. In addition, some smaller *C-shaped* cones are observed to superpose on other larger cones (e.g., Figure S1 in Supporting Information S1), and they are regarded as a part of subjacent larger cones.

Irregular cones: These volcanic cones (Figures 4g and 4h) display irregular and degraded appearances, potentially due to postemplacement impacts or complicated preexisting terrains. Alternatively, their irregular shapes may be caused by multiple eruption phases. We have identified 93 *irregular* cones.

Elongated cones: These volcanic cones (Figures 4i and 4j) display an elongated outline. Their unusually elongated shapes are probably attributed to the sloped preexisting topography, with pyroclastic flowing along the

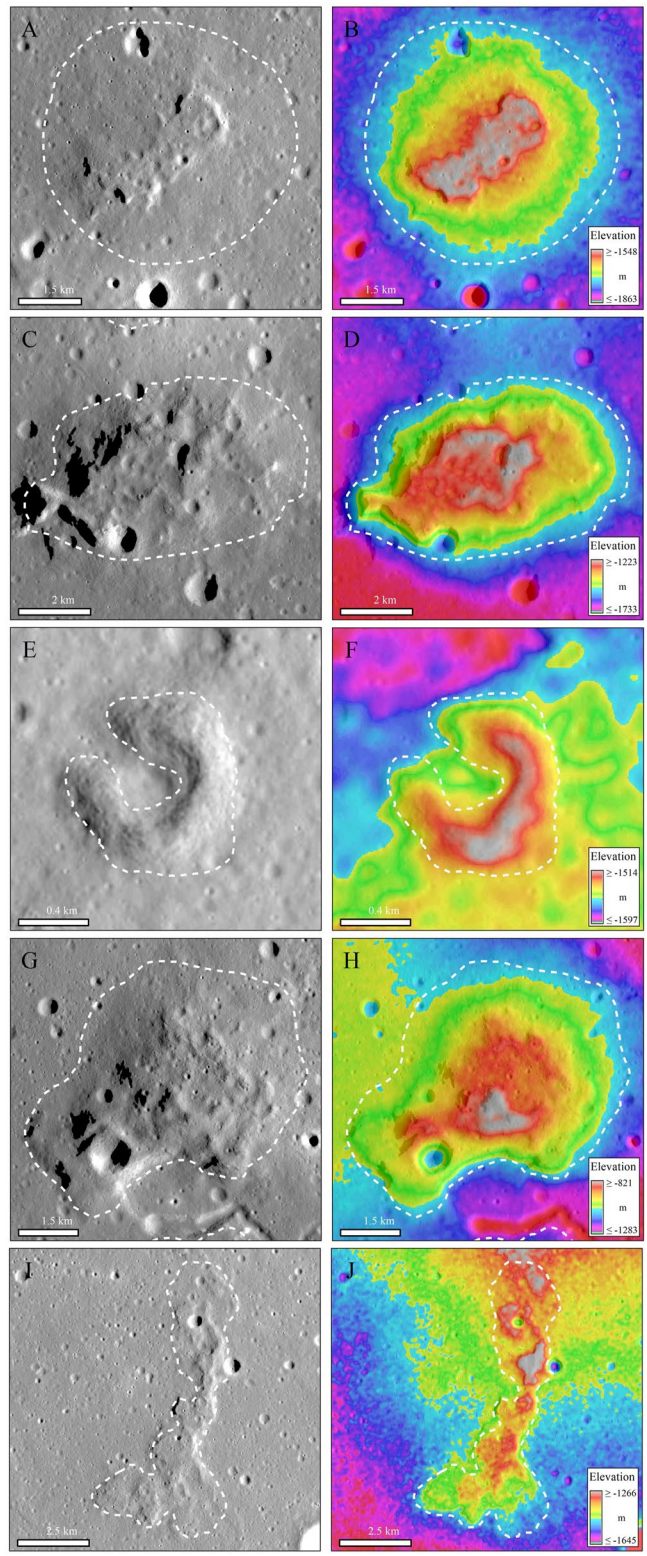


Figure 4. Kaguya Terrain Camera (TC) morning images and Kaguya TC digital terrain model topography maps of representative volcanic cones in Marius Hills: (a, b) A *rounded* cone, located at 11.34°N, 58.22°W, (c, d) an *elliptical* cone, located at 9.91°N, 55.66°W, (e, f) a *C-shaped* cone, located at 15.30°N, 55.24°W, (g, h) an *irregular* cone, located at 14.52°N, 50.10°W, and (i, j) an *elongated* cone, located at 10.13°N, 52.49°W. White dotted lines mark the outline of volcanic cones.

slope. Lawrence et al. (2013) found these cones have an opening containing distinct lava flow channels, an indication of flow emplacement direction. In total, nine elongated cones have been identified.

4.3. Spatial Distribution of Other Volcanic Features in Marius Hills

In addition to volcanic cones, we also identified other volcanic structures in Marius Hills, including sinuous rilles, volcanic domes, and summit pit craters (vents). Similar to the process of the identification of volcanic cones, we also determined the identification, classification, and shape of each dome and summit pit crater. We identified 22 volcanic domes, 61 summit pit craters, and 62 sinuous rilles. Due to the occurrences of apparent flank openings for C-shaped cones, a possible summit pit crater may have been largely deformed or degraded out and beyond recognition. The shape types of domes we recognized only include *elliptical*, *irregular*, and *rounded* domes (Figure 5). No *letter-C or elongated* shapes have been observed for mare domes in Marius Hills. Statistics of the other volcanic structures of different types of classification and shapes are shown in Figures 6b–6d. Detailed information (e.g., latitude and longitude) are compiled in the supplementary materials (Tables S1 and S3 in Supporting Information S1). Compared with the prior survey results of volcanic structures in Marius Hills (more than 150 volcanic domes and 90 cones reported by Lawrence et al. (2013)), the high-resolution and high-altimetric precision of the new data employed in this work enable us to identify more volcanic cones and domes. The spatial distribution of volcanic cones in Marius Hills identified by prior studies and this analysis is compiled in the supplementary materials (Figure S2 in Supporting Information S1).

The spatial distribution of volcanic structures in Marius Hills is mapped in Figure 7a, which shows that cones are widely distributed in Marius Hills and no obvious spatial distribution patterns are observed for volcanic cones with certain shape types. We also calculated the areal density of volcanic cones in a moving circle of 10 km in radius (Figure 7b). Areas with the lowest cone density are generally around the Marius crater and lava flow plains. Regions of significant concentration of cones occur in the northeast and southwest of the Marius Hills plateau, with kernel density up to 0.08 km^{-2}. We found that volcanic cones in the northeast region are mostly *elliptical*, while the volcanic cones in the southwest region are mostly dominated by *C-shaped cones*, indicating possible variations in regional volcanism. In addition, several smaller volcanic cone clusters are identified in the north and west of the Marius Hills and southwest of the Marius crater, with a kernel density of ∼0.04 km^{-2}.

5. Geological Characteristics of Volcanic Cones in Marius Hills

5.1. Dimension

Basal width (W_{co}) and ellipticity are the major morphological parameters for describing the dimension of the volcanic cones in Marius Hills. The frequency distributions of basal width and ellipticity of volcanic cones (Figures 8a and 8b) are characterized by a leptokurtic and unimodal distribution pattern, respectively. The basal width of the majority (335/360 = ∼93%) of volcanic cones in Marius Hills is less than 8 km, with an average value of ∼3.6 km. The ellipticity of cone outlines concentrates between 1 and 1.6.

The frequency distribution pattern varies among cones of different shape types. *C-shaped* cones are all less than 2 km in basal diameter, with relatively low ellipticity. *Elliptical* cones are the most common cones in Marius Hills (n = 151), with a mean basal width of ∼3.3 km. *Elongated* cones are the rarest cones (n = 9), with basal widths up to ∼4 km. Because of its special elongated outline shape, the ellipticities of these cones are the largest (generally larger than 1.7). *Irregular* cones vary widely in basal width (∼0.6–12.6 km) and ellipticity (∼1–2), and they are most common in the 4–6 km basal width range (n = 27 and ∼29% of the cones in this dimension range). Despite their irregular outline shapes, their ellipticities are typically low (<1.2), similar to rounded cones (mean basal width of ∼4.7 km). Some extreme cases of Marius Hills cones, like the largest one (∼14.6 km basal width) at 14.03°N, 49.04°W and the most elongated one (∼4.7 ellipticity) at 16.89° N, 50.91°W, are shown in Figures 8c–8f.

5.2. Height

The frequency distributions of the height and the ratio of height to basal width of volcanic cones with different shape types and the morphometric relationship between height and basal width are shown in Figures 9a–9c.

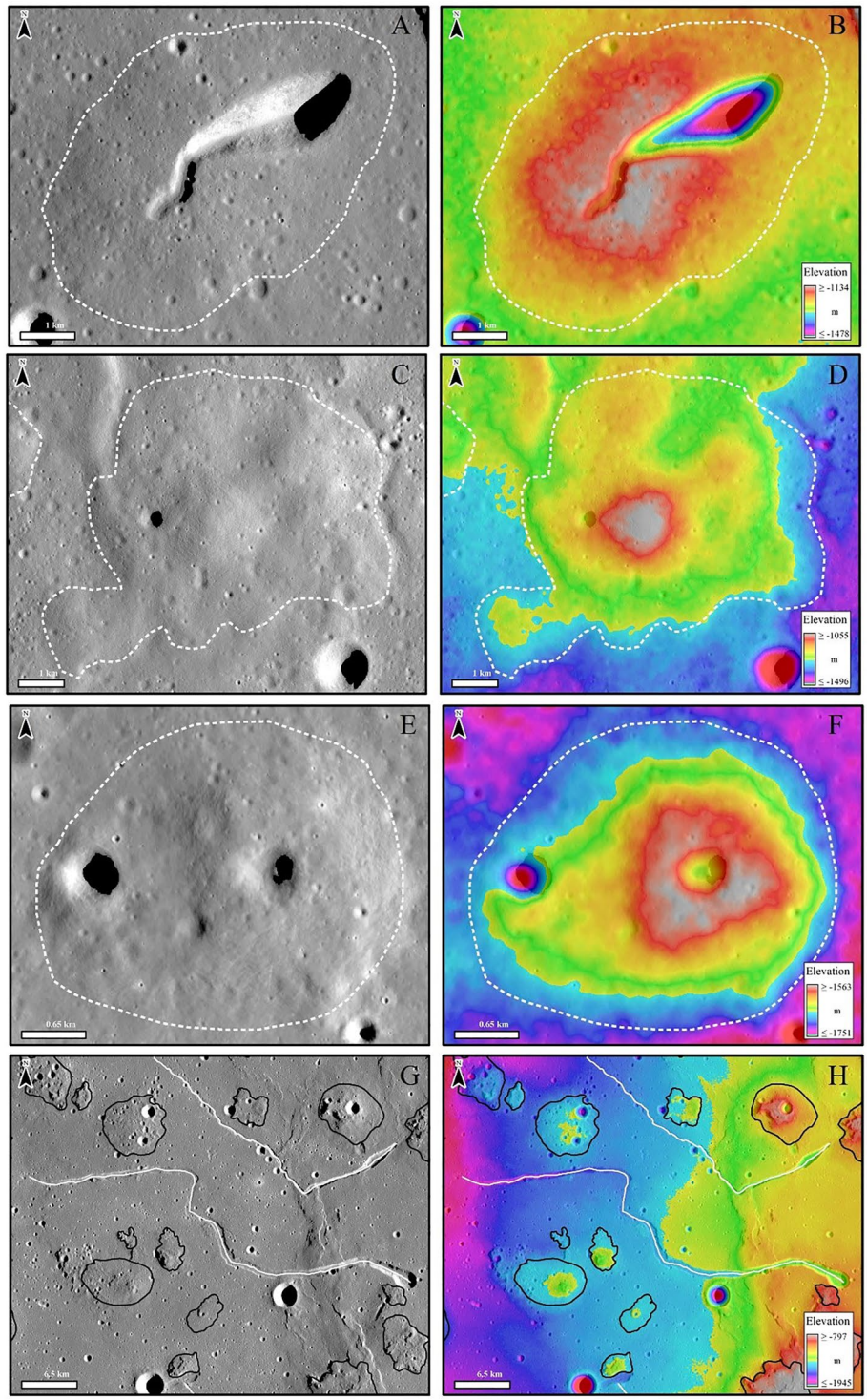


Figure 5. Kaguya Terrain Camera (TC) morning images and Kaguya TC digital terrain model topography maps of other representative volcanic features in Marius Hills: (a, b) An *elliptical* dome, located at 52.45°N, 10.47°W, (c, d) an *irregular* dome, located at 51.42°N, 10.75°W, and (e, f) a *rounded* dome, located at 54.43°N, 9.13°W. The white dotted lines mark the outlines of volcanic cones. (g, h) Two sinuous rilles in the west of the Marius Hills plateau. The white solid lines mark the location of sinuous rilles.

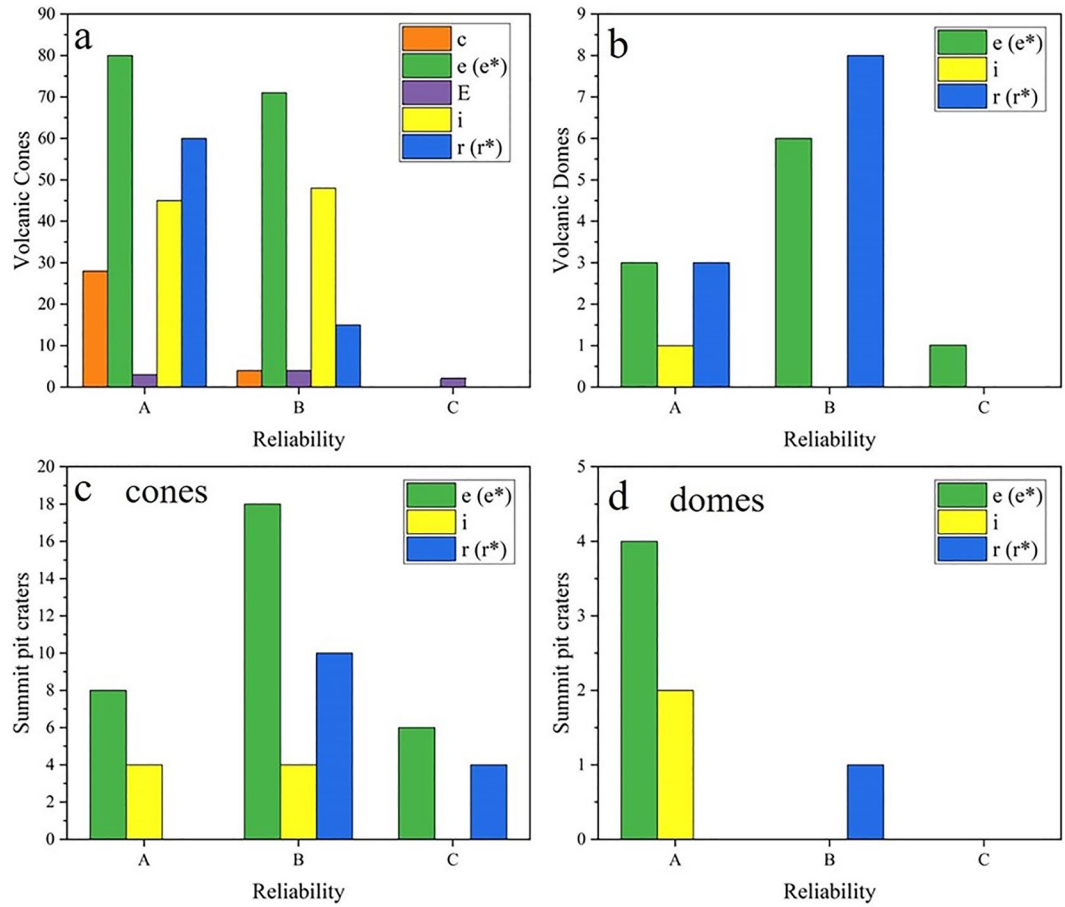


Figure 6. Histograms of (a) volcanic cones, (b) volcanic domes, and (c, d) summit pit craters with different classifications and various shapes ("C" for *C-shaped*, "e" for *elliptical*, "E" for *elongated*, "i" for *irregular*, and "r" for *rounded*).

The heights of volcanic cones in Marius Hills range from ~20 to ~540 m (average value of ~140 m) and are characterized by a leptokurtic distribution pattern, with a peak at ~50–100 m (Figure 9a). The majority (329/360 = ~91%) of these cones are less than 300 m in height. The height/basal width ratios range from ~0.01 to ~0.19 (average value of ~0.05) and show a unimodal distribution. The heights of the Marius Hills cones also vary among cones of different shape types. *C-shaped* cones are generally shorter than 250 m, with relatively greater height/basal width ratios. *Elliptical* cones range widely from ~22 to ~523 m in height, with a median value of around 115 m. *Elongated* cones, despite being much small in population (n = 9), are characterized by a wide range of heights and height/basal width ratios. *Irregular* cones also vary in height, and they (n = ~40) dominate cones shorter than 100 m. Their height/basal width ratios are generally small (<0.05). *Rounded* cones are ~160 m in height on average and show a normal distribution of height/basal width ratios. Cones with maximum height/basal width ratios are usually smaller in size (~1 km basal width) and dominated by a *C-shaped* cone (47.1%), suggesting that smaller cones prefer to retain their initial morphological crispness. Figures 9d–9g shows the highest (~540 m) cone and the cones with the highest height/basal width ratio.

A positive correlation is observed between the cone basal widths and heights (Figure 9c). In addition, cones of different shape types show different trends in the basal width-height plot. Through linear fitting, we identify three possible trends. The first one ($H_{co} = 0.08 \times W_{co}$) only contains *C-shaped* cones, whose heights change most acutely with its basal width. The second one ($H_{co} = 0.03 \times W_{co} + 0.03$) contains *elliptical*, *irregular*, and *rounded* cones, with moderate height/basal width ratios. The third one ($H_{co} = 0.01 \times W_{co} + 0.03$) contains an *elongated* cone, whose heights change the least with its basal width.

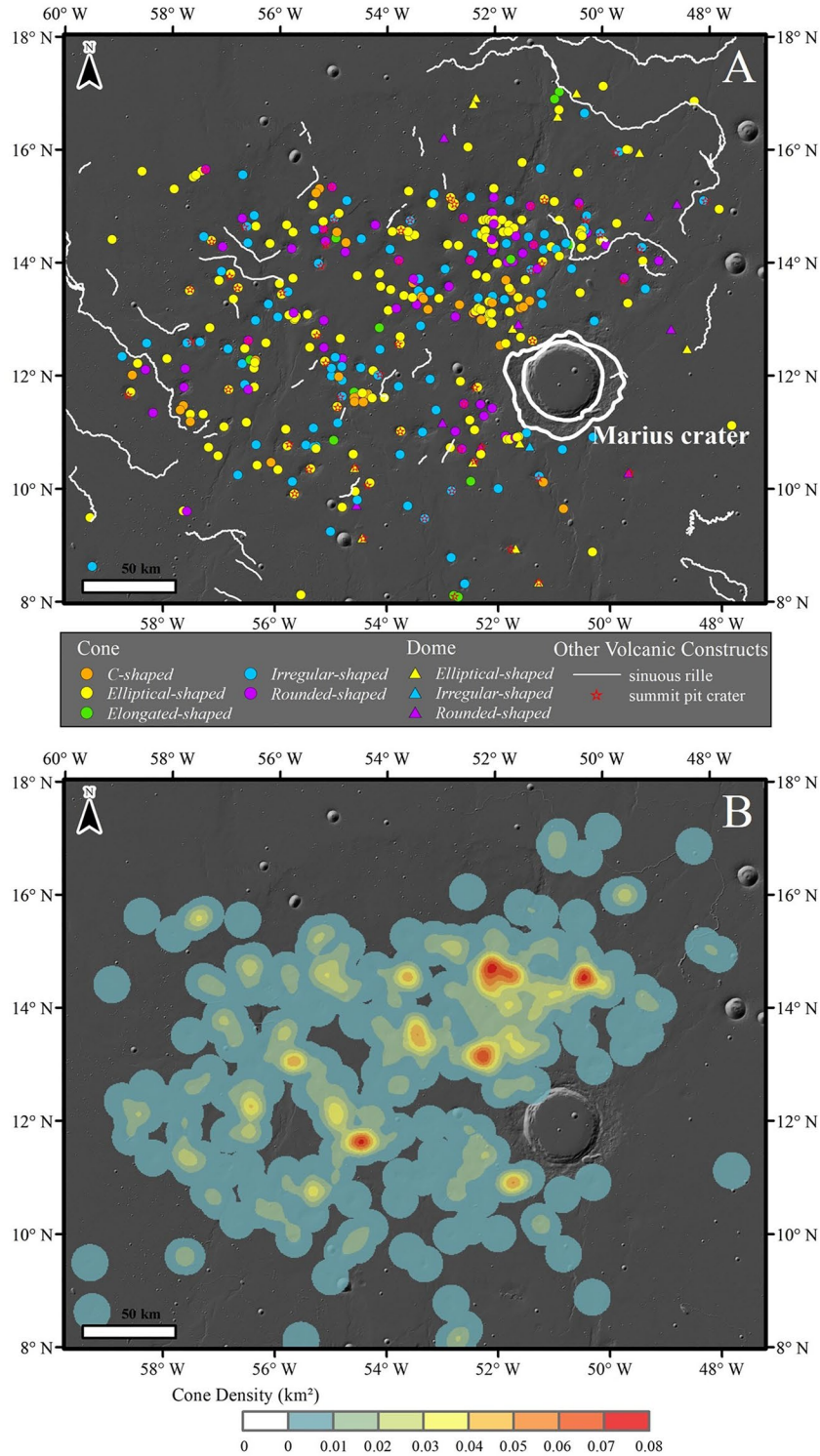


Figure 7. (a) Spatial distribution of volcanic features. (b) Kernel density of volcanic cones (10 km search radius). The base map is a hillshade map transformed from the SLDEM2015 topography.

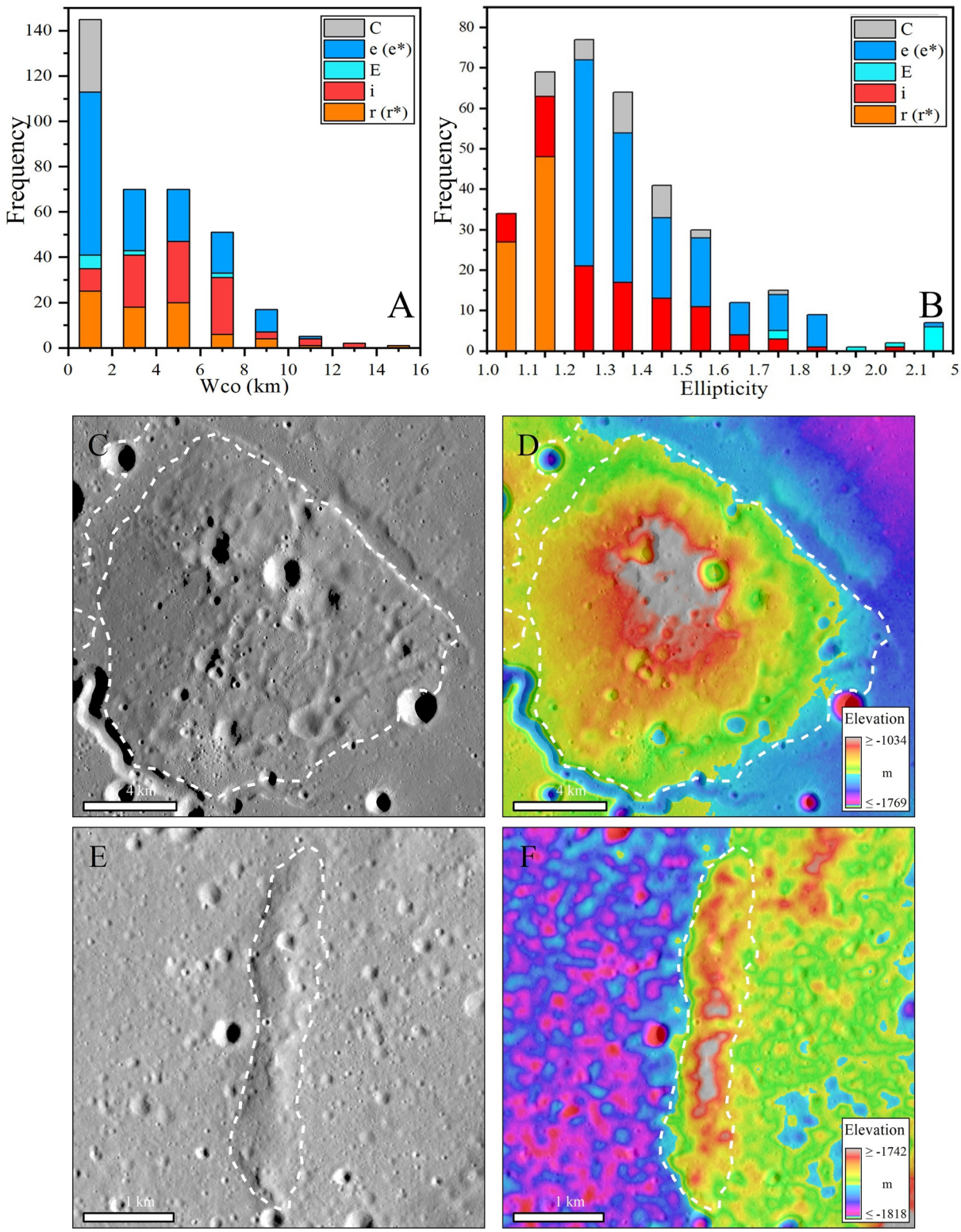


Figure 8. (a, b) Histograms of the basal width and ellipticity of volcanic cones with various shapes. The basal width and ellipticity are measured from Kaguya Terrain Camera (TC) digital terrain model (DTM) topography data. Kaguya TC morning images and Kaguya TC DTM topography maps of cones in Marius Hills: (c, d) The largest (~14.6 km basal width) cone at 14.03°N, 49.04°W, and the most elongated cone (ellipticity = ~4.7) at 16.89° N, 50.91°W. The white dotted lines mark the outlines of volcanic cones.

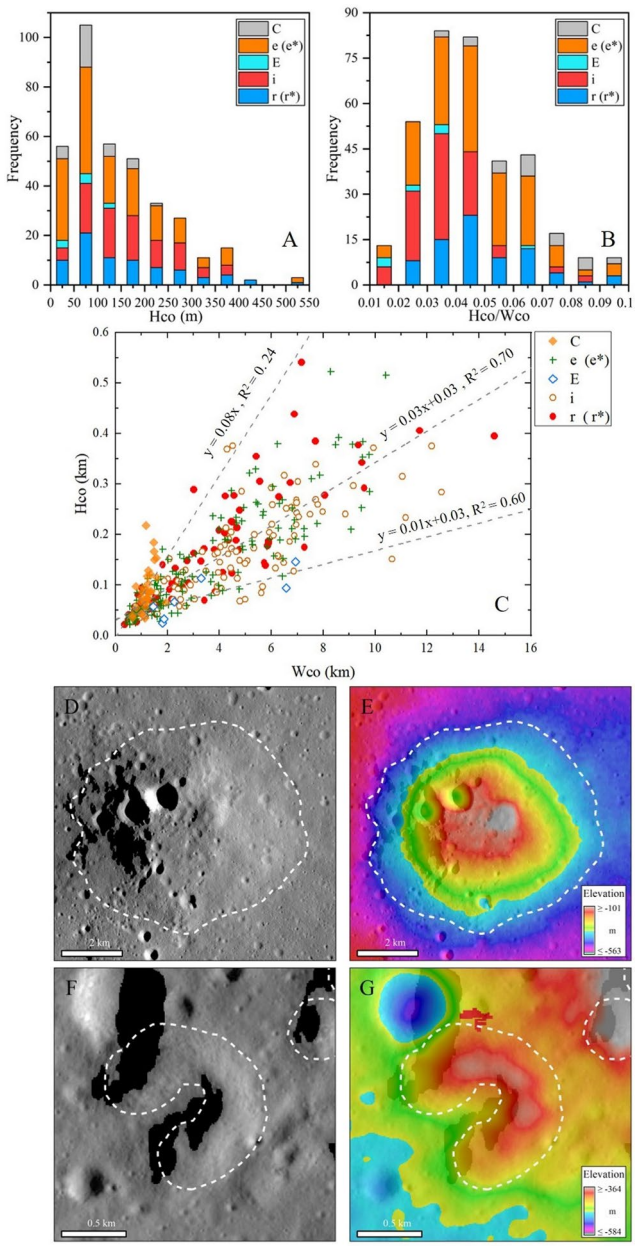


Figure 9. (a, b) Histograms of the height and height/basal width ratio of volcanic cones with various shapes. (c) Scatter plot of the basal width and height of volcanic cones with different shapes. Light gray dotted line: Linear fitting results of *C-shaped* (n = 32), *elliptical*, *irregular,* and *rounded* cones (n = 319), and *elongated* cone (n = 9). The heights are measured from Kaguya Terrain Camera (TC) digital terrain model (DTM) topography data. Kaguya TC morning images and Kaguya TC DTM topography maps of representative cones in Marius Hills: (d, e) The highest cone (~540 m) at 13.58°N, 52.87°W, and (f, g) the cones with the highest height/basal width ratio (~0.19) at 13.10°N, 52.43°W.

5.3. Volume

The volume of volcanic cones in Marius Hills range widely from less than 0.1 to over 10 km^3 (mean value of ~1.55 km^3 and median value of ~0.25 km) and show a positively skewed distribution pattern (Figure 10a). Low-volume cones are much more common than larger cones: The volume for most (280/360 = ~78%) cones is less than 2 km^3. In addition, for cones with a volume <2 km^3, cones are also concentrated in smaller volume ranges, peaking below 0.2 km^3 (Figure 10b). *C-shaped* cones are all smaller than 0.2 km^3 in volume, while cones of other shape types are characterized by a range of volumes, despite small-volume (<0.2 km^3) cones are also much more common. The volume of the volcanic cone is observed to show a power function relationship with basal width (Figure 10c), which can be fitted by an exponential function: Volume = $-2.8 + 2.1^{*}e^{0.18^{*}W_{co}}$ (R^2 = 0.92), where the volume is in km^3 and the basal width is in km.

5.4. Slope

We calculated the topographic slopes of Marius Hills cones from the Kaguya TC DTM topography (with a baseline of 30 m; Figures 11a and 11b), which show that they are generally steeper than mare domes (generally <5°; Qiao, Head, et al., 2021). The mean slopes of Marius Hills cones are characterized by a unimodal distribution pattern, peaking at 5–8° and with a median value of ~7°. The topographic slopes also vary among cones of different shape types. The *C-shaped* cones (mainly ~7–13°) have relatively steeper slopes than cones of other shapes. *Elliptical*, *irregular*, and *rounded* cones show a wide range of mean slopes, with the majority (302/319 = ~95%) having average flank slopes between 5° and 10°. The volcanic cone with the largest mean slope (15.6°) is a *C-shaped* cone located at 13.17°N, 53.26°W (Figure 11c). In addition, smaller cones (basal width <~4 km) are characterized by a wide range of mean topographic slopes (up to ~16°), while larger cones are of relatively steeper slopes (generally <10°). These (generally <2 km) and steep-sloped (6–16° slope) cones are dominated by *C-shaped* cones.

5.5. Rock Abundance

We also characterized the spatial concentrations of surface meter-scale rocks using Diviner thermophysical measurements (Bandfield et al., 2011). Figure 12 shows the general rock abundance in Marius Hills. The overall rock abundance in the study area is small, and the areas with rock abundance above 10% are concentrated in the floors and walls of the impact craters and sinuous rilles in the northeast, while the rock abundance around the volcanic cones and domes is small, basically below 10%. We infer that the slope of the sinuous rilles and crater wall is very steep, and a large number of blocks are caused by mass wasting, which results in the high rock abundance of the sinuous rilles. The low rock abundance of mare may be because of long-term weathering and degradation processes. The mean rock abundance values of Marius Hills cones range from 0.30% to 3.84% (median value ~0.90%) and show a positively-skewed unimodal distribution pattern. Cones of various shape types all show a range of mean RA values, while the majority (304/360 = ~84%) have mean rock abundance between 0.5% and 1.5%. As for the volcanic cones, besides long-term weathering processes, they are composed of pyroclastic rocks with low rock abundance. Elevated rock abundances (>2%) are only observed at some *elliptical* and *rounded* cones, which account for only 2% of the total cone population. The volcanic cone with the largest mean rock abundance (~3.8%) is an *elliptical* cone at 15.12°N, 51.21°W (Figures 13b and 13c). Similar to topographic slopes investigated above, smaller cones have a much wider range of rock abundances than larger cones. In addition, a weak positive correlation between slope and rock abundance is observed, indicating steeper cones are also rockier.

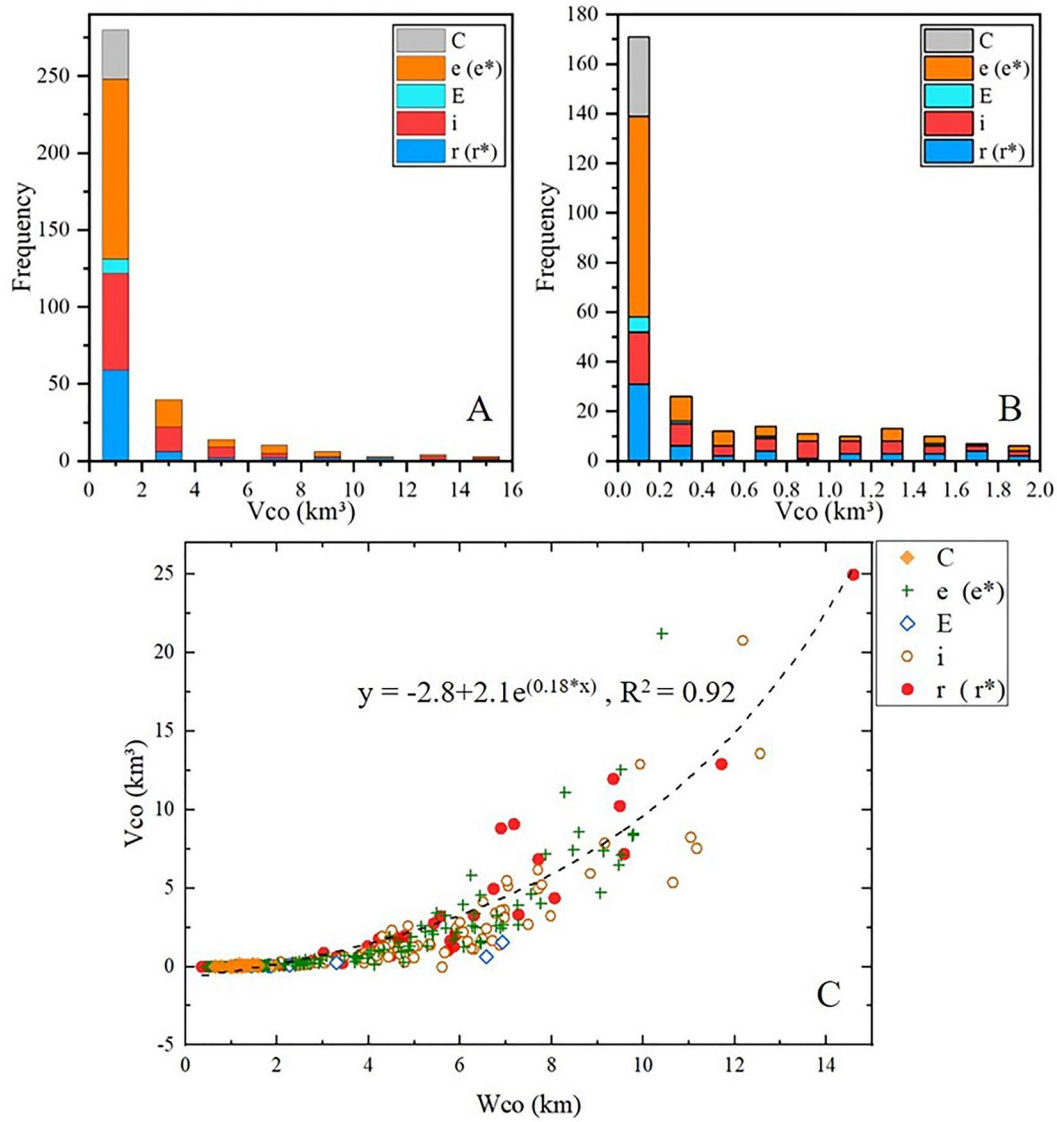


Figure 10. (a) Histogram of the volume of cones with various shapes. (b) The frequency distributions of the volume of volcanic cones with different shapes with volume <0.2 km^3. (c) Scatter plot of the volume and basal width of volcanic cones. The black dotted line is the exponential function fitting curve.

5.6. Summit Pit Craters

Summit pit craters are important components of volcanic cones. We surveyed the occurrence of summit pits at each cataloged cone feature in Marius Hills and found them in 53 (~15%) cones in Marius Hills. The outline shape of the summit pit features is described, including (quasi)-*elliptical*, (quasi)-*irregular*, and (quasi)-*rounded* shapes (Figure 6). Like the procedure for the morphometric analyses of volcanic cones above, we also characterized the width (W_{cr}), depth (D_{cr}), and depth/width ratio (D_{cr}/W_{cr}) of summit pit craters (Figure 14). Detailed information (e.g., latitude and longitude) are compiled in the supplementary materials (Tables S2 and S4 in Supporting Information S1). In general, the histogram of summit pit crater width is characterized by a unimodal distribution pattern, peaking at 200–400 m, with a median value of ~400 m (Figure 14a). The frequency distribution of summit pit crater depths of the Marius Hills cones is positively skewed, concentrating below 40 m, with a median value of ~30 m (Figure 14b). *Elliptical* summit pit craters are characterized by the widest range of width and depth. They also dominate pit craters in the 0.2–0.3 km width range and the shallowest pits (depth <20 m). *Irregular* summit pit craters, despite being the least common shape type for summit pits (8/54 = ~15%), are at the upper end of the width and depth for the entire summit pit population in Marius Hills. *Rounded* summit pit craters

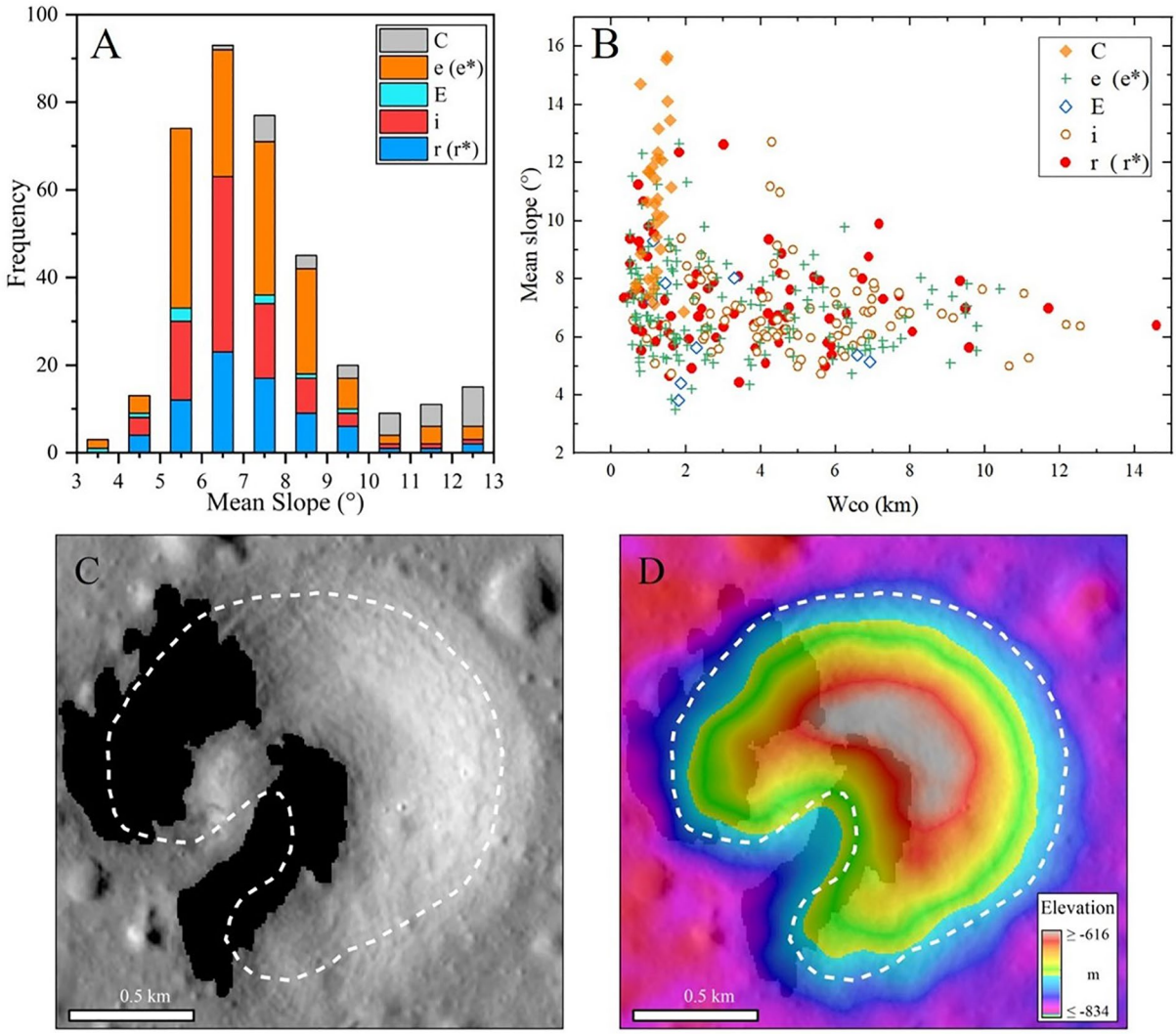


Figure 11. (a) Histogram of the mean slope of volcanic cones with various shapes. (b) Scatter plot of the mean slope-basal width of volcanic cones. (c, d) Kaguya Terrain Camera (TC) morning images and TC digital terrain model topography maps of the steepest (15.6° mean slope) cones at 13.17°N, 53.26°W.

are relatively shallower than other types of summit pits, and most of them (13/14 = ~93%) are <60 m in depth. The largest (~2.1 km width), also the deepest (~0.1 km), summit pit is irregular in shape (located at 11.66°N, 58.68°W, Figures 14c and 14d). The ratio of the summit pit crater width to the volcanic cone basal width varies widely from 0.02 to nearly 0.36, though most of them (47/54 = ~87%) is between 0.03 and 0.2 (Figure 14e). A weak positive correlation is observed between the summit pit width and the cone basal width. The width-depth ratio of most summit pit craters (48/54 = ~89%) is concentrated between 0.04 and 0.15 (Figure 14f), indicating that summit pits atop lunar cones are generally shallower than lunar impact craters (Robbins et al., 2018; Stopar et al., 2017).

6. Discussion

6.1. A Summary of the Morphology of Volcanic Cones in the Marius Hills

Based on our analysis presented above (Sections 4 and 5), the morphology of the volcanic cone population in the Marius Hills has been well constrained (Table 1). Among the cones of various shape types, the *C-shaped* cones are prominent for their small volume (median value ~0.04 km^3) and steepest slope (median value 10.6°). Lawrence et al. (2013) found that the highest elevation along the flank of *C-shaped* cones is in the direction

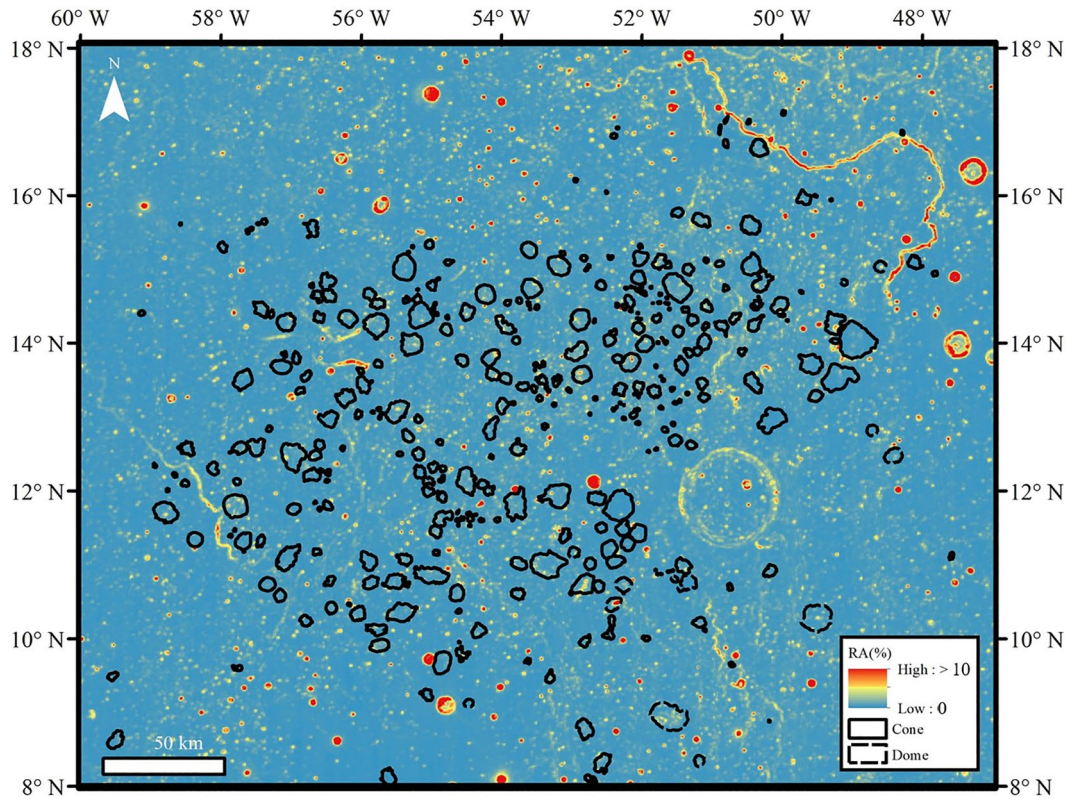


Figure 12. Rock abundance map of the Marius Hills. The outlines of volcanic cones are outlined in black.

opposite to the opening and the flank tilts down toward the opening. We proposed that the *C-shaped* cones are probably *elliptical* or *rounded* cones at the initial building stage while being subject to subsequent breaching by younger radial lava flow from the central vent, and the flank openings are probably the extension of the preexisting summit pit craters.

Elliptical, *irregular*, and *rounded* cones occupy the majority (319/360 = ~89%) of the Marius Hills cone population and all the observed summit pit craters are on cones of these shape types. *Elliptical* and *rounded* cones are of comparable flank slopes (median value of the mean slope of ~7.0°). Both of them represent the majority of well-developed volcanic cones in Marius Hills. The *irregular* cones have the largest size (a median basal width of ~4.5 km, height of ~152 m, and volume of ~1.07 km^3). *Irregular* cones often occur in clusters, and their morphology is affected by preexisting topography or subsequent impacts, which complicates the surface topography and increases partly the size measurement results.

Elongated cones are relatively rare in Marius Hills, while they are characterized by a high ellipticity (median value of ~2.6). We suggest that these elongated cones without associated lava flows are probably formed by the degassing of a near-surfaced dike producing both spatter and volcanic glasses, like the Rima Parry cones (Weitz & Head, 1999).

The range of outline shapes of the Marius Hills cones indicates the variations and complications during the formation and postemplacements of lunar volcanic cones. We suggested that a well-developed cone in flat terrains should be in symmetrical shape (*elliptical* and *rounded*), while they were been modified by many environmental factors to form asymmetrical-shaped cones (*C-shaped*, *irregular*, and *elongated*). The formation and evolution of these asymmetrical cones probably incorporate the following sequences: (a) The heterogeneous eruption and intrusion of pyroclastic and lava around the eruption vent led to the asymmetric structure at the edge of the cone; (b) the preexisting topography makes the lava ejected from the summit crater and flow downhill, which prevents the accumulation of lava and leads to the formation of asymmetric cones; (c) during the formation process, the original symmetrical cone is fragile in a certain direction, because of the further accumulation of lava and pyroclastic, the cone collapsed and rupture in this direction; and (d) The preexisting topography led to the formation

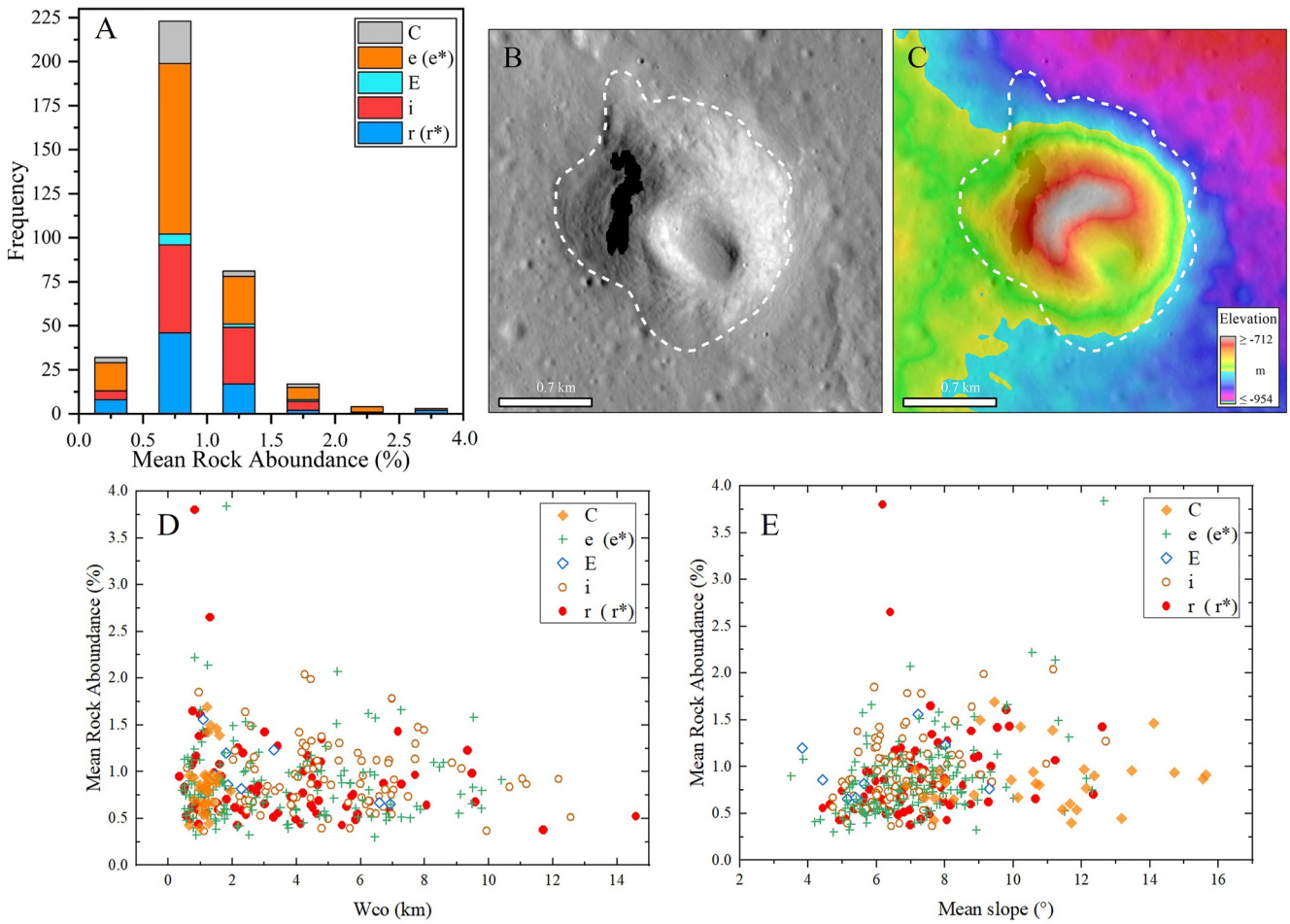


Figure 13. (a) Histogram of the mean rock abundance of volcanic cones with various shapes. (b–c) Kaguya Terrain Camera image and topography maps of the rockiest (3.8% mean rock abundance) at 15.12°N, 51.21°W. Scatter plot of mean rock abundance against (d) the basal width and (e) mean slope of volcanic cones.

of symmetrical volcanic cones, then the lava flowed over the lower position of their edge and accumulated here and gradually eroded to the center of the cone.

6.2. Comparison of the Marius Hills Volcanic Cones and Mare Domes

As typical small-scale volcanic features, mare domes are suitable for comparison with volcanic cones. We identified 22 mare domes in Marius Hills. Similar to our analysis of the Marius Hills cones, the morphology of each dome was also investigated. The basal widths of domes range from ∼1 to ∼13 km, with an average width of 4.1 km, ellipticities range from 1.0 to 1.7 (average value of 1.2), heights range from 0.02 to 0.23 km (average value of 0.09 km), the volume ranges from 0.01 to 10.01 km^3 (average value of 1.12 km^3), and mean slope ranges from 3.3° to 8.7° (average value of 5.0°). Summit pit craters were found in ∼32% (7/22) of the Marius Hills domes. Compared with volcanic cones in Marius Hills, mare domes are relatively large in basal width, gentle in flank, and rounded in outline shape. The Marius Hills cones have smaller basal widths, suggesting the low-volume and small-scale eruptions for the formation of lunar volcanic cones (Figure 15). In addition, the W_{cr}/W_{co} ratio of the Marius Hills cones is less than that of the mare dome, indicating a lower degree of caldera collapse during the cone-building eruptions.

6.3. Comparison With Terrestrial Volcanic Cones

The ratio between the summit pit crater width and the volcanic constructs basal width is an informative indicator of the particle size, vent width, gas content of magma, eruption rate, constancy of eruption, and the crater collapse

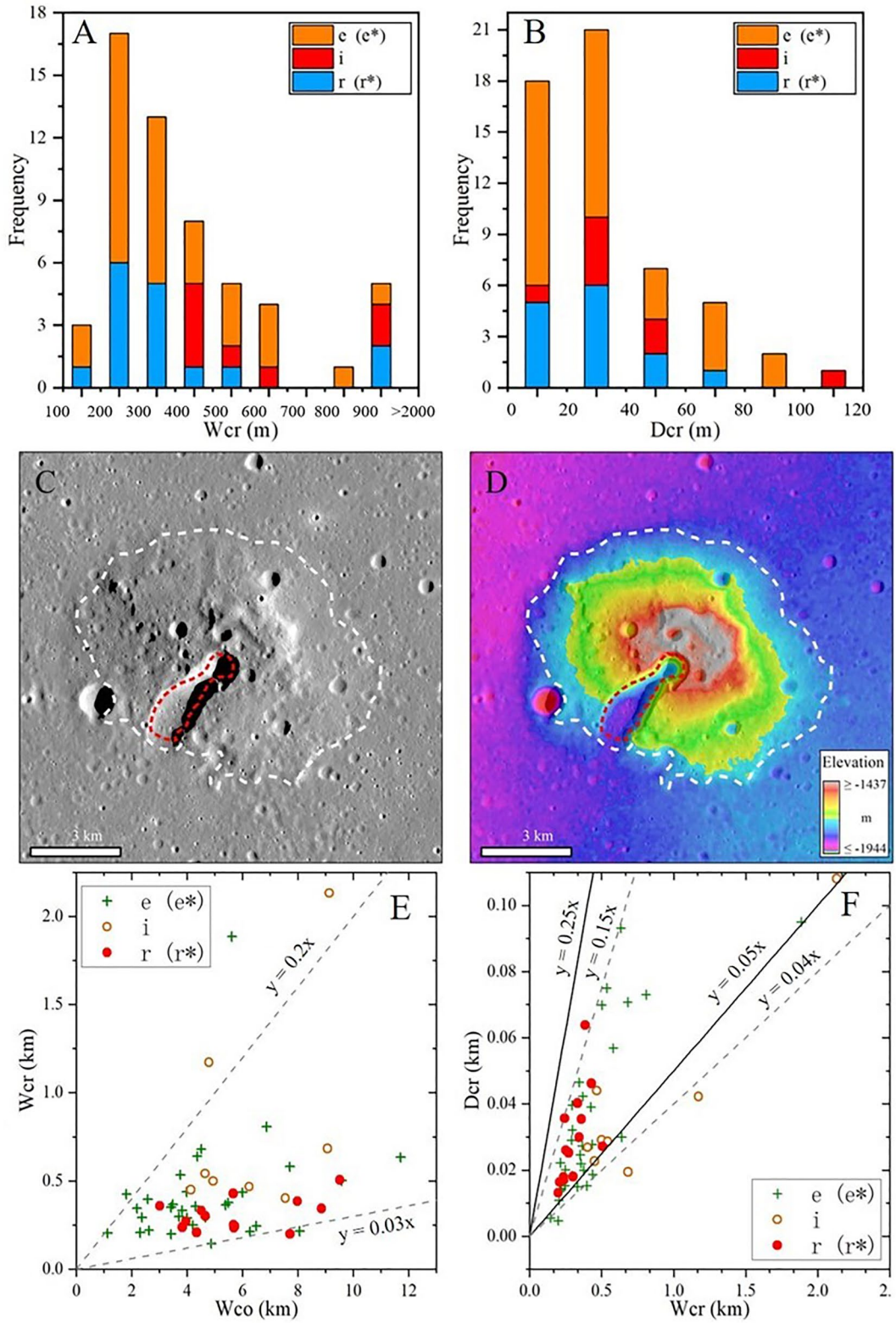


Figure 14. (a) Histograms of the width and depth of summit pit crater of volcanic cones with various shapes. (c, d) Kaguya Terrain Camera image and topography maps of the largest (~2.1 km width) and deepest (~0.1 km) summit pit crater in Marius Hills (11.66°N, 58.68°W). Scatter plot of the summit pit crater width against the (e) cone basal width and (f) summit pit crater depth.

Table 1
The Median Value of Morphological Parameters of Cataloged Volcanic Cones in Marius Hills

Shape category					
Morphological parameters	C-shaped	Elliptical	Elongated	Irregular	Rounded
Basal width (km)	1.2	2.2	1.9	4.5	3.3
Ellipticity	1.2	1.4	2.6	1.3	1.1
Height (m)	87	100	66	152	139
Volume (km^3)	0.04	0.15	0.05	1.07	0.54
Mean slope (°)	10.6	7.0	5.6	6.6	7.0
Mean rock abundance (%)	0.85	0.80	0.86	0.87	0.74

process (Head, 1975; Head & Gifford, 1980; Wilson & Head, 1981; Wood, 1979). Prior studies have reported some W_{cr}/W_{co} ratio values for certain types of volcanic features. The W_{cr}/W_{co} ratio is observed to be around 0.4, 0.36, 0.08, and 0.12 for fresh terrestrial cinder cones, spatter cones, low shield volcanoes, and steep shield volcanoes, respectively (Porter, 1972; Wood, 1979, 1980). While viscous terrestrial lava domes have a very high W_{cr}/W_{co} ratio of around 0.4–0.7. The W_{cr}/W_{co} ratio of terrestrial stratovolcanoes and shield volcanoes ranges from 0.05 to 0.2 (Smith, 1973). Volcanic cones in Marius Hills have a mean W_{cr}/W_{co} ratio of ~0.1, which is much smaller than terrestrial cones but comparable with terrestrial shield volcanoes.

Another key morphological ratio used to quantify the shape of volcanic cones is the cone height to basal width ratio (H_{co}/W_{co}). For cone fields at Mauna Kea and Lanzarote, Kervyn et al. (2012) found that the H_{co}/W_{co} ratios of cones in Mauna Kea and Lanzarote are from 0.06 to 0.2 and 0.04 to 0.2, respectively. Some linear functions are also proposed previously for terrestrial cones, for instance, $H_{co} = 0.18W_{co}$ (Porter, 1972) or $H_{co} = 0.20W_{co}$ (Settle, 1979). In comparison, volcanic cones in Marius Hills show a wide range of H_{co}/W_{co} ratio values (Figure 16), suggesting variations in the formation process of lunar cones of different types. Whereas, more than half (209/360 = ~58%) of the Marius Hills cones have H_{co}/W_{co} ratios within the range of terrestrial cones (Kervyn

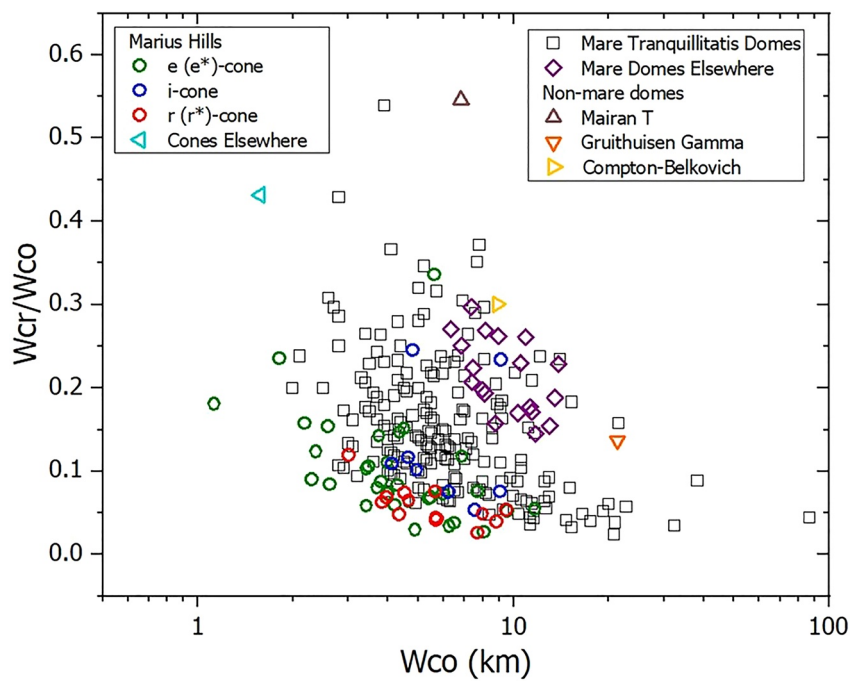


Figure 15. Scatter plot of the summit pit crater basal width to volcanic construct basal width ratio against the basal width. Morphological parameters of lunar cones, mare domes, and nonmare domes elsewhere are from Lawrence et al. (2013), Chauhan et al. (2015), and Qiao, Head, et al. (2021).

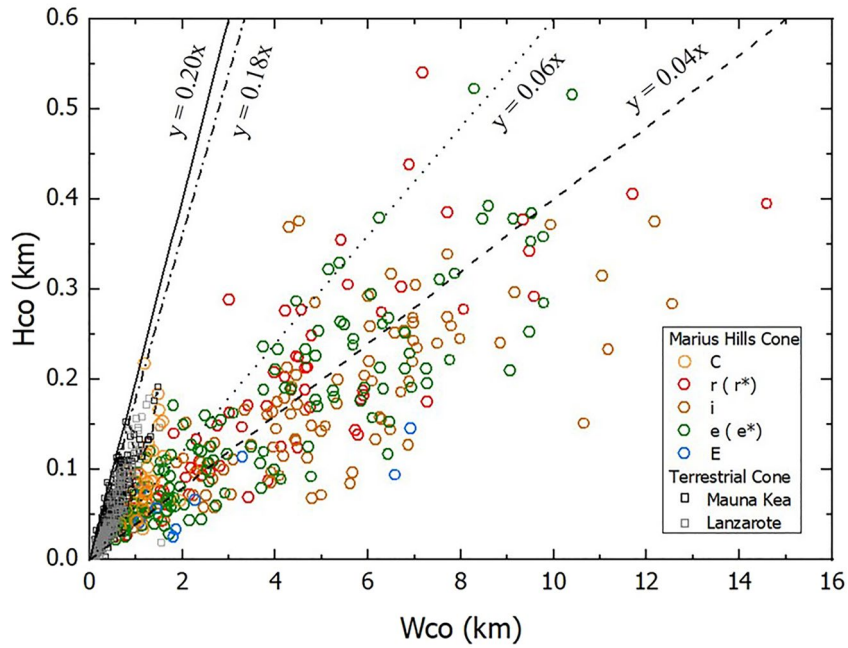


Figure 16. Scatter plot of the volcanic cone height-basal width with various shapes. Dash-dotted line: $H_{co} = 0.18W_{co}$ (Porter, 1972), bold line: $H_{co} = 0.20W_{co}$ (Settle, 1979), dotted line: Minimum ratio for simple unbreached cones in Mauna Kea, and dashed line: Minimum ratio for simple unbreached cones in Lanzarote (Kervyn et al., 2012).

et al., 2012), although the lunar volcanic cones are larger and higher, demonstrating some morphological similarities between lunar and terrestrial volcanic cones.

As illustrated by Mcgetchin and Head (1973), the formation of terrestrial cinder cones generally incorporates four stages of processes: Low-rimmed pyroclastic ring, development of exterior talus, destruction of the original rim, and the growth of cone beyond the ballistic limit of ejecta. According to the geomorphic observations of the volcanic cones in Marius Hills, most of them are probably at the first stage. Under lunar environments of low gravity and the absence of an atmosphere, the ejecting time of pyroclastics is predicted to be longer, resulting in larger basal width than that of terrestrial eruptions. The basal width distribution ranges of the lunar cone and terrestrial cone are 0–12 and 0–2 km respectively (Figure 16), consistent with the effect of gravity difference between the Earth and the Moon.

6.4. Implications for the Origin of Volcanic Cones in Marius Hills

According to the dike propagation theory proposed by Head and Wilson (2017), lunar volcanic cones originate from the strombolian eruption. During the expansion of the dike, the volatiles in the magma are dissolved and gradually gathered at the top of the dike. When the dike reaches the lunar surface, the pressure difference between the magma bubbles and lunar surface environments (nearly vacuum) makes the magma burst from the fissures on the lunar surface, which forms the corresponding volcanic formations dominated by volcanic cones. On the whole, the Marius Hills are a large volcanic rise, and the surrounding mare unit is the product of volcanic activity in Marius Hills, which to some extent reflects the activity of volcanism in the study area and the underground magma reservoirs. We infer that most of the volcanic cones in the Marius region are the products of small-volume and volatile-rich volcanic activities after large-scale volcanic activities. Therefore, compared with previous studies, we have identified more volcanic cones and fewer domes. In addition, the single peak distribution characteristics of volcanic cones' morphological parameters found in Section 5 also reflect the similarity of magma eruption flux, magma physical properties, volatile content, and lunar surface environments. Whereas, whether there is a complex but uniform network of dike systems under the Marius Hills deserves further in-depth analysis.

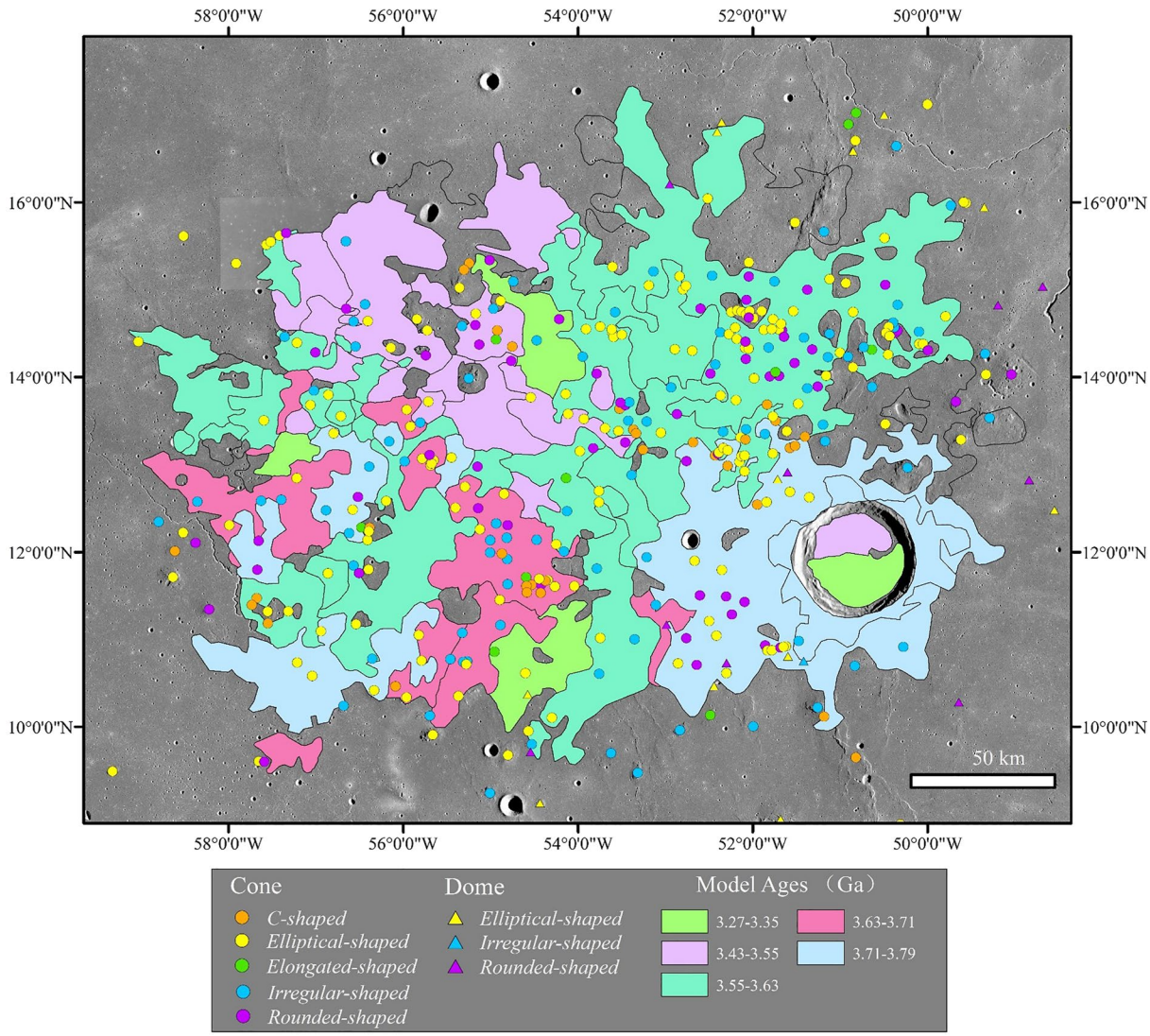


Figure 17. Spatial distribution of volcanic structures in the map of model ages of the Marius Hills (Imaeda et al., 2013).

6.5. The Model Ages of the Volcanic Cones in Marius Hills

The stratigraphy and chronology of the Marius Hills volcanic features and deposits have also been studied previously. McCauley (1967) and Wilhelms and McCauley (1971) mapped the Marius Hills as Eratosthenian-aged. Huang et al. (2011) report crater size-frequency distribution (CSFD) absolute model ages for Marius basalts, medium to low titanium basalt, and undifferentiated medium titanium basalt, and the results are 814, 949, and 687 Ma, respectively. The spatial distribution of volcanic structures in the map of model ages of the Marius Hills (Huang et al., 2011) is compiled in the supplementary materials (Figure S3 in Supporting Information S1). Most recently, Imaeda et al. (2013) calculated the model ages of the Marius Hills based on the Kaguya TC data and found that their ages range from 3.3 to 3.8 Ga (Figure 17). The significant age disparity between the two studies is likely attributed to the variations in the geological unit definition, size and locations of the crater count working area, the employed image data, diameter range and numbers of the crater for age fitting, and measurement variations between different investigators, as seen in many lunar surfaces dating studies, for instance, the Chang'e-5 sampling area dating results (Qiao, Xu, et al., 2021). We used the dating results of Imaeda et al. (2013) to investigate the chronologies of volcanic cones in Marius Hills. We found that the earlier volcanic activities (3.71–3.79 Ga) occurred around the Marius crater in the southeast of Marius Hills, during which many *elliptical* and *rounded* cones were formed. Frequent volcanic activities occurred in the northeast and southwest of the

Marius Hills (also the area with the highest density of volcanic cones, Figure 7b) at the age of 3.55–3.71 Ga. The majority of the *irregular* and *elliptical* cones were formed during this period. The late phase of regional volcanism (3.27–3.55 Ga) in Marius Hills mainly occurs in the northwest portion and crater floor of the Marius floor and abundant cones of various shape types were formed. It is worth noting that the age of the Marius floor unit differs greatly from that of the surrounding mare units. On the one hand, the volcanic units around the Marius crater may be older due to the impact of resurfacing process. On the other hand, there was a small-scale young volcanic activity on the Marius floor. Besse et al. (2011) proposed that the floor filling of the Marius crater is the result of the latest volcanic episode of the Marius Hills, which is an important part of understanding volcanism in Marius Hills.

7. Conclusions

This paper focuses on the volcanic cone and related volcanic formations in the Marius Hills. We conducted a comprehensive search campaign for volcanic cones in the Marius Hills using multisource remote sensing data to carry out identification, classification, and morphological parameter calculation. It provides a certain understanding of lunar volcanic activity from the aspect of morphology. The main conclusions are as follows:

1. The identification and classification of the volcanic cones and related volcanic formations in Marius Hills.

Based on the topographic data sets, 360 volcanic cones and 22 mare domes were identified in the Marius Hills. Compared with the latest survey results of volcanic structures in Marius Hills (Lawrence et al., 2013), the new data with high spatial resolution and altimetric precision enable us to identify more volcanic cones. According to the morphological characteristics, the volcanic cones in the Marius Hills can be divided into five categories: *C-shaped*, *elliptical*, *elongated*, *irregular*, and *rounded* cones. The spatial distribution of various volcanic cones is mapped, which shows that the volcanism in Marius Hills is concentrated in the northeast and southwest portions.

2. Morphological analysis of the Marius Hills volcanic cones.

Using the Kaguya TC DTM topography, morphological parameters and morphological ratios were calculated to constrain the morphology of the cones in Marius Hills. In the aspects of dimension, height, volume, slope, and rock abundance, various types of volcanic cones are well distinguished. The range of outline shapes of the Marius Hills cones is probably attributed to the variations and complications during the formation and postemplacements of lunar volcanic cones, with symmetrical cones (*elliptical* or *rounded*) formed in the initial phases, which were then heavily modified and formed asymmetrical cones (*C-shaped* or *irregular*).

3. Comparison of the Marius Hills volcanic cones with domes and terrestrial volcanic cones.

Compared with mare domes elsewhere on the Moon, Marius Hills volcanic constructs tend to have smaller basal width and smaller summit pit crater basal width, suggesting the low-volume and small-scale eruptions for the formation of lunar volcanic cones. Compared with terrestrial volcanic cones, the Marius Hills volcanic cones have larger basal widths but smaller H_{co}/W_{co} ratios, which are mainly attributed to unique lunar environments of low gravity and the absence of an atmosphere.

4. Time sequence of volcanism in Marius Hills.

The earlier volcanic activity in Marius Hills occurred in the southeast of the Marius Hills, during which the *elliptical* and *rounded* cones were formed. Multiphase volcanic activities occurred in the northeast and southwest of the Marius region and formed the majority of the *irregular* and *elliptical* cones. The last phase of volcanism in Marius Hills mainly occurred in the northwest and Marius floor, during which cones of various morphology types formed.

In summary, the Marius Hills area of the Moon is a volcanic "hotspot" with abundant volcanic structures. These cones are thought to be pyroclasts formed at the terminal stage of regional volcanic activity. The differences in morphology between volcanic cones imply the diversity of volcanic eruptions in various periods. The measurement and analysis of their morphology will help us to further explore the history of lunar volcanism.

Data Availability Statement

The LRO LROC low-Sun mosaics can be found at the LROC Data Node Reduced Data Records (https://pds.lroc.asu.edu/data/LRO-L-LROC-5-RDR-V1.0/), the SLDEM2015 data are archived at the PDS Geosciences Node (https://pds-geosciences.wustl.edu/lro/lro-l-lola-3-rdr-v1/lrolol_1xxx/data/sldem2015/), the Kaguya TC image data are available from the SELENE Data Archive (https://data.darts.isas.jaxa.jp/pub/pds3/sln-l-tc-5-morning-map-v4.0/), and the Kaguya topography data are available from the SELENE Data Archive (https://data.darts.isas.jaxa.jp/pub/pds3/sln-l-tc-5-dtm-map-seamless-v2.0/). Derived data in Tables S1–S4 in Supporting Information S1 are accessible at Zenodo (Wan, 2022).

Acknowledgments
This research was funded by the National Natural Science Foundation of China, Grant 41972322, 11941001, and U1931211; preresearch project on Civil Aerospace Technologies funded by China National Space Administration (CNSA), Grant D020102 and D020204; the Project of China Geological Survey, Grant DD20221645; National Key Research and Development Program of China, Grant 2020YFE0202100 and 2019YFE0123300; Natural Science Foundation of Shandong Province, Grant ZR2019MD008; Key Research Program of Frontier Sciences, CAS, Grant QYZDY-SSW-DQC028; Strategic Priority Research Program of Chinese Academy of Sciences, Grant XDB 41000000; and Young Scholars Program of Shandong University, Weihai (No. 202207).

References

Arya, A. S., Rajasekhar, R. P., Amitabh, Gopala Krishna, B., Ajai, & Kiran Kumar, A. (2014). Morphometric, rheological and compositional analysis of an effusive lunar dome using high-resolution remote sensing data sets: A case study from Marius hills region. *Advances in Space Research*, *54*(10), 2073–2086. https://doi.org/10.1016/j.asr.2013.10.014

Bandfield, J. L., Ghent, R. R., Vasavada, A. R., Paige, D. A., Lawrence, S. J., & Robinson, M. S. (2011). Lunar surface rock abundance and regolith fines temperatures derived from LRO Diviner Radiometer data. *Journal of Geophysical Research*, *116*(E12), E00H02. https://doi.org/10.1029/2011je003866

Barker, M., Mazarico, E., Neumann, G., Zuber, M., Haruyama, J., & Smith, D. (2016). A new lunar digital elevation model from the lunar orbiter laser altimeter and SELENE terrain camera. *Icarus*, *273*, 346–355. https://doi.org/10.1016/j.icarus.2015.07.039

Besse, S., Sunshine, J., Staid, M., Petro, N. E., Boardman, J. W., Green, R. O., et al. (2011). Compositional variability of the Marius hills volcanic complex from the Moon Mineralogy Mapper (M3). *Journal of Geophysical Research*, *116*(E6), E00G13. https://doi.org/10.1029/2010je003725

Chauhan, M., Bhattacharya, S., Saran, S., Chauhan, P., & Dagar, A. (2015). Compton–Belkovich volcanic complex (CBVC): An ash flow caldera on the Moon. *Icarus*, *253*, 115–129. https://doi.org/10.1016/j.icarus.2015.02.024

Earle, S. (2019). 4.3 Types of volcanoes. In *Physical geology* (2nd ed.).

Greeley, R. (1971). Lava tubes and channels in the lunar Marius Hills. *The Moon*, *3*(3), 289–314. https://doi.org/10.1007/bf00561842

Grosse, P., De Vries, B. V. W., Euillades, P. A., Kervyn, M., & Petrinovic, I. A. (2012). Systematic morphometric characterization of volcanic edifices using digital elevation models. *Geomorphology*, *136*(1), 114–131. https://doi.org/10.1016/j.geomorph.2011.06.001

Guest, J., & Murray, J. (1976). Volcanic features of the nearside equatorial lunar maria. *Journal of the Geological Society*, *132*(3), 251–258. https://doi.org/10.1144/gsjgs.132.3.0251

Guest, J. E. (1971). Centres of igneous activity in the maria. In *Geology and physics of the Moon. A study of some fundamental problems* (pp. 41–53).

Haruyama, J., Hara, S., Hioki, K., Iwasaki, A., Morota, T., Ohtake, M., et al. (2012). Lunar global digital terrain model dataset produced from SELENE (Kaguya) terrain camera stereo observations. In *Lunar and planetary science conference* (p. 1200).

Head, J. (1975). Morphology of pyroclastic lunar volcanic deposits: Implications for eruption conditions and localized sources of volatiles. In *Lunar and planetary science conference*.

Head, J. W., & Gifford, A. (1980). Lunar mare domes: Classification and modes of origin. *The Moon and the Planets*, *22*(2), 235–258. https://doi.org/10.1007/bf00898434

Head, J. W., & Wilson, L. (2017). Generation, ascent and eruption of magma on the Moon: New insights into source depths, magma supply, intrusions and effusive/explosive eruptions (Part 2: Predicted emplacement processes and observations). *Icarus*, *283*, 176–223. https://doi.org/10.1016/j.icarus.2016.05.031

Heather, D. J., Dunkin, S. K., & Wilson, L. (2003). Volcanism on the Marius Hills plateau: Observational analyses using Clementine multispectral data. *Journal of Geophysical Research*, *108*(E3), 5017. https://doi.org/10.1029/2002je001938

Huang, J., Xiao, L., He, X., Qiao, L., Zhao, J., & Li, H. (2011). Geological characteristics and model ages of Marius Hills on the Moon. *Journal of Earth Sciences*, *22*(5), 601–609. https://doi.org/10.1007/s12583-011-0211-8

Imaeda, R., Haruyama, J., Ohtake, M., Iwata, T., Arimoto, T., Ito, K., et al. (2013). Lunar Marius Hills plateau exhibiting the early Imbrian model age. In *44th annual lunar and planetary science conference* (p. 1503).

Kervyn, M., Ernst, G., Carracedo, J.-C., & Jacobs, P. (2012). Geomorphometric variability of "monogenetic" volcanic cones: Evidence from Mauna Kea, Lanzarote and experimental cones. *Geomorphology*, *136*(1), 59–75. https://doi.org/10.1016/j.geomorph.2011.04.009

Lawrence, S. J., Stopar, J. D., Hawke, B. R., Greenhagen, B. T., Cahill, J. T. S., Bandfield, J. L., et al. (2013). LRO observations of morphology and surface roughness of volcanic cones and lobate lava flows in the Marius Hills. *Journal of Geophysical Research-Planets*, *118*(4), 615–634. https://doi.org/10.1002/jgre.20060

McCauley, J. F. (1967). *Geologic map of the Hevelius region of the Moon*. US Geological Survey Report (p. 491).

McCauley, J. F. (1968). Geologic results from the lunar precursor probes. *AIAA Journal*, *6*(10), 1991–1996. https://doi.org/10.2514/3.4912

Mcgetchin, T. R., & Head, J. W. (1973). Lunar cinder cones. *Science*, *180*(4081), 68–71. https://doi.org/10.1126/science.180.4081.68

Nelson, D., Koeber, S., Daud, K., Robinson, M. S., Watters, T. R., Banks, M. E., et al. (2014). Mapping lunar maria extents and lobate scarps using LROC image products. In *Lunar and planetary science conference* (p. 2861).

Poldervaart, A. (1971). *Volcanicity and forms of extrusive bodies, volcanic landforms and surface features* (pp. 1–18). Springer.

Porter, S. C. (1972). Distribution, morphology, and size frequency of cinder cones on Mauna Kea volcano, Hawaii. *The Geological Society of America Bulletin*, *83*(12), 3607–3612. https://doi.org/10.1130/0016-7606(1972)83[3607:dmasfo]2.0.co;2

Qiao, L., Head, J. W., Wilson, L., Chen, J., & Ling, Z. (2021). Mare domes in mare tranquillitatis: Identification, characterization, and implications for their origin. *Journal of Geophysical Research: Planets*, *126*(9), e2021JE006888. https://doi.org/10.1029/2021je006888

Qiao, L., Xu, L., Yang, Y., Xie, M., Chen, J., Fang, K., & Ling, Z. (2021). Cratering records in the Chang'e-5 mare unit: Filling the "age gap" of the lunar crater chronology and preparation for its re-calibration. *Geophysical Research Letters*, *48*(22), e2021GL095132. https://doi.org/10.1029/2021GL095132

Robbins, S. J., Watters, W. A., Chappelow, J. E., Bray, V. J., Daubar, I. J., Craddock, R. A., et al. (2018). Measuring impact crater depth throughout the solar system. *Meteoritics & Planetary Sciences*, *53*(4), 583–637. https://doi.org/10.1111/maps.12956

Scholten, F., Oberst, J., Matz, K. D., Roatsch, T., Wahlisch, M., Speyerer, E. J., & Robinson, M. S. (2012). GLD100: The near-global lunar 100 m raster DTM from LROC WAC stereo image data. *Journal of Geophysical Research*, *117*(E12), E00H17. https://doi.org/10.1029/2011je003926

Settle, M. (1979). The structure and emplacement of cinder cone fields. *American Journal of Science*, *279*(10), 1089–1107. https://doi.org/10.2475/ajs.279.10.1089

Smith, E. I. (1973). Identification, distribution, and significance of lunar volcanic domes. *The Moon*, *6*(1), 3–31. https://doi.org/10.1007/bf02630650

Stopar, J. D., Robinson, M. S., Barnouin, O. S., McEwen, A. S., Speyerer, E. J., Henriksen, M. R., & Sutton, S. S. (2017). Relative depths of simple craters and the nature of the lunar regolith. *Icarus*, *298*, 34–48. https://doi.org/10.1016/j.icarus.2017.05.022

Sunshine, J., Pieters, C., Head, J., McEwen, A. S., & Greeley, R. (1992). Oceanus Procellarum as viewed by Galileo: Evidence for compositional diversity in the mare deposits and at the Marius Hills Plateau. In *Lunar and planetary science conference*.

Thouret, J. C. (1999). Volcanic geomorphology—An overview. *Earth-Science Reviews*, *47*(1–2), 95–131. https://doi.org/10.1016/s0012-8252(99)00014-8

Wan, S. (2022). Volcanic cones in the Marius hill [Dataset]. Zenodo. https://doi.org/10.5281/zenodo.6704459

Weitz, C. M., & Head III, J. W. (1999). Spectral properties of the Marius Hills volcanic complex and implications for the formation of lunar domes and cones. *Journal of Geophysical Research*, *104*(E8), 18933–18956. https://doi.org/10.1029/1998je000630

Whitford-Stark, J. L., & Head, J. W. (1977). The Procellarum volcanic complexes—Contrasting styles of volcanism. In *Lunar and planetary science conference proceedings* (pp. 2705–2724).

Whitford-Stark, J. L., & Head III, J. W. (1980). Stratigraphy of Oceanus Procellarum basalts: Sources and styles of emplacement. *Journal of Geophysical Research*, *85*(B11), 6579–6609. https://doi.org/10.1029/jb085ib11p06579

Wilhelms, D. E., & McCauley, J. F. (1971). *Geologic map of the near side of the Moon*. US Geological Survey.

Wilson, L., & Head III, J. W. (1981). Ascent and eruption of basaltic magma on the Earth and Moon. *Journal of Geophysical Research*, *86*(B4), 2971–3001. https://doi.org/10.1029/jb086ib04p02971

Wood, C. A. (1979). Monogenetic volcanoes of the terrestrial planets. In *Lunar and planetary science conference proceedings* (pp. 2815–2840).

Wood, C. A. (1980). Morphometric evolution of cinder cones. *Journal of Volcanology and Geothermal Research*, *7*(3–4), 387–413. https://doi.org/10.1016/0377-0273(80)90040-2